ATLAS NOTE

ATLAS-CONF-2013-062

June 23, 2013

Search for squarks and gluinos in events with isolated leptons, jets and missing transverse momentum at $\sqrt{s} = 8$ TeV with the ATLAS detector

The ATLAS Collaboration

Abstract

This note presents a search for supersymmetry by the ATLAS experiment at the LHC in final states containing at least one isolated lepton (electron or muon), jets, with or without b-jet requirements, and large missing transverse momentum. The kinematic reach of the analysis is extended to soft leptons to increase the sensitivity to supersymmetric spectra with small mass splitting. The search is based on the proton-proton collision data at a center-of-mass energy $\sqrt{s} = 8$ TeV collected in 2012, corresponding to an integrated luminosity of 20 fb^{-1}. No significant excess above the Standard Model expectation is observed. The results are used to set limits on sparticle masses for various simplified models covering the pair production of gluinos, first and second generation squarks and top squarks. Limits are also set on a MSUGRA/CMSSM model and on the parameters of a minimal Universal Extra Dimensions model.

ATLAS-CONF-2013-062
25 June 2013

1 Introduction

Supersymmetry (SUSY) [1–9] has been proposed as a theory that could describe physical phenomena beyond the Standard Model (SM). It postulates the existence of SUSY particles which differ by half a unit of spin with respect to that of their SM partner. The squarks ($\tilde{q}$) and sleptons ($\tilde{\ell}$) are the scalar partners of the quarks and leptons, the gluinos ($\tilde{g}$) are the fermionic partners of the gluons, and the charginos ($\tilde{\chi}_i^{\pm}$ with $i = 1, 2$) and neutralinos ($\tilde{\chi}_j^0$ with $j = 1, 2, 3, 4$), are the mass eigenstates formed from the linear superpositions of the SUSY partners of the Higgs and electroweak gauge bosons.

If strongly interacting supersymmetric particles are present at the TeV-scale, they should be accessible at the Large Hadron Collider [10]. In the minimal supersymmetric extension of the Standard Model [11–15] such particles decay into jets, possibly leptons and the lightest supersymmetric particle (LSP). The LSP is stable, owing to R-parity conservation, and can be weakly interacting and therefore escape detection, leading to missing transverse momentum ($\boldsymbol{p}_{\mathrm{T}}^{\mathrm{miss}}$ and its magnitude $E_{\mathrm{T}}^{\mathrm{miss}}$) in the final state. Significant $E_{\mathrm{T}}^{\mathrm{miss}}$ can also arise in R-parity violating scenarios in which the LSP decays to final states containing neutrinos or in scenarios where neutrinos are present in the cascade decay.

This note presents a search with the ATLAS detector for SUSY in final states containing jets, possibly identified as originating from b-quarks (b-jets), at least one isolated lepton (electron or muon) and large $E_{\mathrm{T}}^{\mathrm{miss}}$. The search probes events characterized by the presence of a low ($10(6) < p_{\mathrm{T}} < 25$ GeV) or of a high ($p_{\mathrm{T}} > 25$ GeV) transverse momentum electron (muon). In the following, the former class of events is referred to as the soft-lepton channel, the latter as the hard-lepton channel. Previous searches in this channel have been conducted by the ATLAS [16] and CMS [17] collaborations using their full 2011 dataset at a center-of-mass energy of 7 TeV. The ATLAS collaboration has also conducted a search in the final state containing four high transverse momentum jets, large missing transverse momentum and one isolated hard lepton for a 5.8 fb^{-1} subset of the 2012 dataset at $\sqrt{s} = 8$ TeV [18]. In this note, the analysis is reported with the full 2012 dataset at a center-of-mass energy of 8 TeV. The analysis is extended to also search for direct top squark pair production and minimal Universal Extra Dimensions (mUED). Ten different signal regions are used in this search, all optimized for the new center-of-mass energy and the full 2012 dataset.

2 The ATLAS Detector

The ATLAS detector [19, 20] consists of a tracking system (inner detector, or ID) surrounded by a thin superconducting solenoid providing a 2 T magnetic field, electromagnetic and hadronic calorimeters and a muon spectrometer (MS). The ID consists of pixel and silicon microstrip detectors, surrounded by the transition radiation tracker (TRT). The electromagnetic calorimeter is a lead liquid-argon (LAr) detector. Hadron calorimetry is based on two different detector technologies, with scintillator-tiles or LAr as active media, and with either steel, copper, or tungsten as the absorber material. The MS is based on three large superconducting toroids arranged with an eight-fold azimuthal coil symmetry around the calorimeters, and a system of three stations of chambers for the trigger and for precise measurements. The nominal pp interaction point at the center of the detector is defined as the origin of a right-handed coordinate system. The positive x-axis is defined by the direction from the interaction point to the center of the LHC ring, with the positive y-axis pointing upwards, while the beam direction defines the z-axis. The azimuthal angle ϕ is measured around the beam axis and the polar angle θ is the angle from the z-axis. The pseudorapidity is defined as $\eta = -\ln\tan(\theta/2)$.

3 SUSY Signal Modeling and Simulated Event Samples

Simulated event samples are used for estimating the signal acceptance, the detector efficiency, and to aid in the estimation of SM background contributions.

3.1 Signal Event Samples

The signal models considered here are the pair production of first and second generation squarks, top squarks and gluinos, each covered by different simplified models [21, 22], a MSUGRA/CMSSM model [23, 24] and the mUED model [25].

The first type of simplified models focuses on the pair production of gluinos or of left-squarks, the latter assuming degenerate first and second generation squarks. This category of models is subdivided into three different decay chains: the "one-step" models, "two-step" models with sleptons and "two-step" models without sleptons. In the "one-step" models, the pair-produced strongly interacting sparticles decay via the lighter chargino, considered to be a pure wino, into a W and the lightest neutralino, considered to be a pure bino. The free parameters in these models are the mass of the gluino/squark and either the mass of the chargino, with a fixed LSP mass set at 60 GeV, or the mass of the LSP, with the chargino mass sitting halfway between the gluino/squark mass and the LSP mass. These one-step models are also studied in the ATLAS analysis based on jets and large missing transverse momentum [26]. In the "two-step" models with sleptons, the strongly interacting sparticles decay with equal probability to either the lighter chargino or the next-to-lightest neutralino. These subsequently decay via left-sleptons (or sneutrinos) which decay into a lepton (neutrino) and the lightest neutralino. In these models, the free parameters are the initial sparticle mass and the LSP mass. The masses of the intermediate charginos/neutralinos are equal and set to be exactly halfway between the gluino/squark and LSP masses, while the slepton and sneutrino masses (all lepton flavours are considered to be mass degenerate) are set exactly halfway between the intermediate chargino/neutralino masses and the LSP mass. Finally, in the "two-step" models without sleptons, the initial sparticle decays via the lighter chargino which itself decays into a W-boson and the next-to-lightest neutralino. The latter finally decays into a Z-boson and the LSP. The lighter chargino mass sits exactly halfway between the gluino/squark mass and the LSP mass. The next-to-lightest neutralino mass is set to be exactly halfway between the lighter chargino mass and the LSP mass. This signature could be realized in the Minimal Supersymmetric Standard Model in a parameter region where additional decay modes, not contained in the simplified model, may lead to a significant reduction of the cross section times branching fraction of the WZ signature.

The second type of simplified models considered in this analysis targets a "natural" SUSY scenario [27, 28] in which at least one top squark and higgsinos are light. In this scenario, the lightest neutralino and chargino are higgsino-like and almost degenerate in mass. The lightest top squark is pair-produced. In the simplified scenario considered here, it then decays exclusively into the lighter chargino and a b-quark; the chargino itself then decays into the lightest neutralino via an off-shell W-boson. Two values of the mass difference between the lighter chargino and the LSP are studied: 5 and 20 GeV. The remaining free parameters in this model are the mass of the top squark and the mass of the LSP. Only models compatible with the chargino mass limit of 103.5 GeV set by the LEP experiments [29] are explored. These top squark models are also studied in the ATLAS analysis based on two b-jets and missing transverse momentum [30]. The analysis presented here is complementary in that the soft-lepton channels focus on scenarios where the top squark – LSP mass difference is small (below 100 GeV) to moderate (on the order of 200 GeV).

In these simplified models, all the sparticles which do not directly enter the production and decay chain are effectively decoupled and are given a mass of 4.5 TeV. The simplified models are generated with one extra jet in the matrix element using MadGraph5 [31], interfaced to PYTHIA [32], and parton density functions (PDFs) from CTEQ6L1 [33]; MLM matching [34] is done with a scale parameter that

is set to a quarter of the mass of the lightest sparticle in the hard-scattering matrix element. The ATLAS underlying event tune AUET2 is used [35].

The MSUGRA/CMSSM model considered in this analysis, defined by $\tan\beta = 30$, $A_0 = -2m_0$ and $\mu > 0$, is compatible with a lightest scalar Higgs boson mass of approximately 125 GeV in most of its parameter space in m_0 and $m_{1/2}$. These samples are generated with Herwig++ [36]. SUSY-HIT [37] interfaced to SOFTSUSY [38] and SDECAY [39] are used to calculate the sparticle mass spectra and decay tables, and to ensure consistent electroweak symmetry breaking in the MSUGRA/CMSSM models.

This analysis also considers the mUED model, which is the minimum extension of the SM with one additional universal spatial dimension. The properties of the model depend on only three parameters [25]: the compactification radius R, the cut-off Λ and the Higgs boson mass m_h. In this model, the mass spectrum is naturally degenerate and the Kaluza-Klein (KK) quark decay chain to the lightest KK particle, the KK-photon, gives a signature very similar to the supersymmetric decay chain of a squark to the lightest neutralino. Signal events for this model are generated with a fixed Higgs mass of 125 GeV using Herwig++ [36] with PDFs from CTEQ6L1 [33] and the CTEQ6L1-UE-EE-3 tune [40]. This model is also studied in the ATLAS analysis based on jets and large transverse missing momentum [26].

For the simplified models and the MSUGRA/CMSSM model, the signal cross sections are calculated at next-to-leading order (NLO) in the strong coupling constant, adding the resummation of soft gluon emission at next-to-leading-logarithmic accuracy (NLO+NLL) [41–45]. The nominal cross section and the uncertainty are taken from an envelope of cross section predictions using different PDF sets and factorisation and renormalisation scales, as described in Ref. [46]. For the mUED model, the cross section is taken at leading order from Herwig++.

3.2 Standard Model Event Samples

The simulated event samples for the SM backgrounds are summarized in Table 1. The ALPGEN [49] samples are generated with the MLM matching scheme. HERWIG [60] is used for simulating the parton shower and fragmentation processes in combination with JIMMY [61] for underlying event simulation for the MC@NLO [54] and the ALPGEN samples. PYTHIA [32] is used for the MadGraph5 [31], POWHEG [50] and AcerMC [52] samples. The PDFs used in this analysis are CTEQ6L1 [33] for the ALPGEN, MadGraph and AcerMC samples and CT10 [62] for the MC@NLO, SHERPA [47] and POWHEG samples. The ATLAS underlying event tune AUET2 is used [35]. SHERPA uses its own parton shower, fragmentation and underlying event model. The SHERPA W+jets and Z/γ^*+jets samples are generated with massive b/c-quarks to improve the description of the b-tagging variables. The soft-lepton channels, which have signal regions with b-jets, therefore use the SHERPA samples which are more appropriate, while the hard-lepton channels use ALPGEN instead for which larger samples were produced at high jet multiplicity. The high-mass SHERPA or ALPGEN Z/γ^*+jets samples are denoted Z+jets background throughout this note, while the low-mass ALPGEN Z/γ^* + jets samples are denoted Drell-Yan.

The theoretical cross sections for W+jets and Z+jets are calculated with DYNNLO [63] with the MSTW2008NNLO [64] PDF set. The diboson cross sections are obtained from MCFM [57]. The $t\bar{t}$ cross section is calculated with HATHOR 1.2 [51] using MSTW2008NNLO PDFs. The single-top cross sections are computed at NLO+NLL accuracy [53, 55, 56] and the $t\bar{t} + W/Z$ cross sections, at NLO accuracy [58, 59].

Physics process	Generator	Cross section (pb)	Cross section calculation	
Soft-lepton analyses				
$W(\rightarrow \ell\nu)$ + jets	SHERPA 1.4.1 [47]	1.22×10^4	NNLO	[48]
$Z/\gamma^*(\rightarrow \ell\ell)$ + jets ($m_{\ell\ell} > 40$ GeV)	SHERPA 1.4.1 [47]	1.24×10^3	NNLO	[48]
$Z/\gamma^*(\rightarrow \ell\ell)$ + jets ($10 < m_{\ell\ell} < 40$ GeV)	ALPGEN 2.14 [49]	4.27×10^3	NNLO	[48]
Hard-lepton analyses				
$W(\rightarrow \ell\nu)$ + jets	ALPGEN 2.14 [49]	1.22×10^4	NNLO	[48]
$W(\rightarrow \ell\nu) + b\bar{b}$ + jets	ALPGEN 2.14 [49]	153	LO×K	
$W(\rightarrow \ell\nu) + c\bar{c}$ + jets	ALPGEN 2.14 [49]	461	LO×K	
$W(\rightarrow \ell\nu) + c$ + jets	ALPGEN 2.14 [49]	1.29×10^3	LO×K	
$Z/\gamma^*(\rightarrow \ell\ell)$ + jets ($m_{\ell\ell} > 60$ GeV)	ALPGEN 2.14 [49]	1.15×10^3	NNLO	[48]
$Z/\gamma^*(\rightarrow \ell\ell)$ + jets ($10 < m_{\ell\ell} < 60$ GeV)	ALPGEN 2.14 [49]	4.37×10^3	NNLO	[48]
$Z/\gamma^*(\rightarrow \ell\ell) + b\bar{b}$ + jets ($m_{\ell\ell} > 60$ GeV)	ALPGEN 2.14 [49]	15.2	NNLO	[48]
All analyses				
$t\bar{t}$	POWHEG r1556 [50]	238	NLO+NLL	[51]
Single-top (t-chan)	AcerMC 3.8 [52]	9.46	NLO+NLL	[53]
Single-top (s-chan)	MC@NLO 4.06 [54]	0.61	NLO+NLL	[55]
Single-top (Wt-chan)	MC@NLO 4.06 [54]	22.4	NLO+NLL	[56]
WW	SHERPA 1.4.1 [47]	5.88	NLO	[57]
WZ	SHERPA 1.4.1 [47]	10.34	NLO	[57]
ZZ	SHERPA 1.4.1 [47]	10.26	NLO	[57]
$W\gamma$	SHERPA 1.4.1 [47]	96.9	LO	
$Z\gamma$	SHERPA 1.4.1 [47]	488	LO	
$t\bar{t} + W$	MadGraph5 [31]	0.232	NLO	[58]
$t\bar{t} + Z$	MadGraph5 [31]	0.208	NLO	[59]

Table 1: Simulated background event samples used in this analysis, and the production cross sections. The ALPGEN W + light jet samples are generated with $0 \leq N_{\text{parton}} \leq 6$ in the matrix element, the ALPGEN Z + light jet samples, with $0 \leq N_{\text{parton}} \leq 5$, the ALPGEN heavy-flavour samples, with $N^{\text{max}}_{\text{parton}} = 3$, except $W + c$, for which $N^{\text{max}}_{\text{parton}} = 4$. The cross section values shown for the W + light jets, the Z/γ^* + light jets, the $Z/\gamma^* + b\bar{b}$ and the single-top (in the s- and $t-$ channels) are listed for a single lepton flavour. The notation LO×K indicates that the process is calculated at leading-order and corrected by a factor derived from the ratio of NLO to LO cross sections for a closely related process. Details of PDF sets and underlying event tunes are given in the text.

3.3 Simulation

The detector simulation is performed either with a full ATLAS detector simulation [65] based on Geant4 [66] or a fast simulation based on the parameterization of the performance of the ATLAS electromagnetic and hadronic calorimeters [67]. All simulated samples are generated with a range of simulated minimum-bias interactions overlaid on the hard-scattering event to account for the multiple pp interactions in the same bunch crossing (pile-up). The overlay also treats the impact of pile-up on bunch crossings other than the one in which the event occurred. Simulated samples are corrected by taking into account the observed differences between the data and simulation for the lepton trigger and reconstruction efficiencies, and for the efficiency and misidentification rate of the algorithm used to identify jets arising from b-quarks (b-tagging).

4 Trigger and Data Collection

The data used in this analysis were collected in 2012 during which the instantaneous luminosity of the LHC reached $7.7\times10^{33}\text{cm}^{-2}\text{s}^{-1}$. The average number of expected interactions per bunch crossing ranged from approximately 6 to 40. After the application of beam, detector, and data-quality requirements, the total integrated luminosity is 20.1 fb^{-1} in the soft-lepton channels and 20.3 fb^{-1} in the hard-lepton channels; the integrated luminosity differs as these channels use different trigger requirements. The uncertainty on the integrated luminosity is ±2.8%. It is derived, following the same methodology as that detailed in Ref. [68], from a preliminary calibration of the luminosity scale derived from beam-separation scans performed in November 2012.

In the hard single-electron channel, a combined electron+$E_{\text{T}}^{\text{miss}}$ trigger is used, with thresholds at 24 GeV for the electron and 35 GeV for $E_{\text{T}}^{\text{miss}}$. The $E_{\text{T}}^{\text{miss}}$ trigger uses a local hadronic calibration for the clusters and is fully efficient for $E_{\text{T}}^{\text{miss}}>$ 80 GeV. The electron trigger selects events containing one or more electron candidates, based on the presence of a cluster in the electromagnetic calorimeter, with a shower shape consistent with that of an electron and is fully efficient for electron p_{T} above 25 GeV.

In the hard single-muon channel, a combined muon+jet+$E_{\text{T}}^{\text{miss}}$ trigger is used, with thresholds at 24 GeV for the muon, 65 GeV for the jet and 40 GeV for $E_{\text{T}}^{\text{miss}}$. The muon trigger selects events containing one or more muon candidates based on the hit patterns in the MS and ID. The trigger reaches its maximal efficiency for calibrated offline jets with $p_{\text{T}}>$80 GeV, muons satisfying $p_{\text{T}}>$25 GeV and $E_{\text{T}}^{\text{miss}}>$ 100 GeV.

With the thresholds on single and dilepton triggers being too high to be suitable for the soft-lepton event selections, these channels rely on a $E_{\text{T}}^{\text{miss}}>$ 80 GeV trigger which is fully efficient in events having a jet with $p_{\text{T}}>$60 GeV and $E_{\text{T}}^{\text{miss}}>$ 150 GeV.

As the hard-lepton searches are based on triggers which depend on the lepton flavour, the electron and muon channels are treated independently in these searches, while the soft-lepton searches, based on a $E_{\text{T}}^{\text{miss}}$ trigger, treat them jointly.

5 Object Reconstruction

This analysis is based on five categories of event selection:

1. A “hard single-lepton channel” to search for the pair production of gluinos or first and second generation squarks.

2. A “soft single-lepton channel” geared towards the same production as the hard single-lepton channel, but optimized for compressed spectra.

3. A “soft dimuon channel” whose target is the mUED model.

4. A "soft single-lepton one b-jet channel" requiring one b-jet to cover the top squark pair production where the mass difference between the top squark and the LSP is small.

5. A "soft single-lepton two b-jet channel" requiring two b-jets to cover the top squark pair production for which the mass difference between the top squark and the LSP is moderate.

In this Section, the final-state object reconstruction and selection requirements are described. The event selection requirements will be described in detail in Section 6.

5.1 Object preselection

The primary vertex [69] is required to be consistent with the beamspot envelope and to have at least five tracks; when more than one such vertex is found, the vertex with the largest summed $|p_{\mathrm{T}}|^2$ of the associated tracks is chosen.

Jets are reconstructed from three-dimensional calorimeter energy clusters using the anti-k_{t} algorithm [70, 71] with a radius parameter $R = 0.4$. Jets arising from detector noise, cosmic rays or other non-collision sources are rejected [72]. To take into account the differences in calorimeter response between electrons/photons and hadrons, each cluster is classified, prior to the jet reconstruction, as coming from an electromagnetic or hadronic shower on the basis of its shape [20]. The jet energy is then corrected at cluster level by weighting electromagnetic and hadronic energy deposits with correction factors derived from Monte Carlo simulation. A further calibration, relating the response of the calorimeter to true jet energy [72, 73], is then applied to the jet energy. "Preselected" jets are required to have $p_{\mathrm{T}} > 20$ GeV.

Electrons are reconstructed from clusters in the electromagnetic calorimeter matched to a track in the ID [74]. The "preselected" electrons are required to pass a variant of the "medium" selection of [74], which has been modified in 2012 to reduce the impact of pile-up [75]. These electrons must have, in the soft(hard)-lepton channels, $p_{\mathrm{T}} > 7$ (10) GeV, $|\eta| < 2.47$ and a distance to the closest preselected jet of $\Delta R < 0.2$ or $\Delta R > 0.4$, where $\Delta R = \sqrt{(\Delta\eta)^2 + (\Delta\phi)^2}$. Electrons with $\Delta R < 0.2$ are kept, and the jet is discarded. Any event containing a preselected electron in the electromagnetic calorimeter transition region, $1.37 < |\eta| < 1.52$, is rejected.

Muons are identified either as a combined track in the MS and ID systems, or as an ID track matching with a MS segment [76,77]. Requirements on the quality of the ID track are identical to those in Ref. [78]. "Preselected" muons in the soft(hard)-lepton channels are required to have $p_{\mathrm{T}} > 6$ (10) GeV, $|\eta| < 2.4$ and $\Delta R > 0.4$ with respect to the closest preselected jet.

The missing transverse momentum calculation uses calorimeter clusters calibrated according to the reconstructed physics object to which they are associated. The association is performed with well-identified objects (electrons, photons, jets and muons). The remaining non-associated energy deposits are also taken into account using an energy-flow algorithm [79].

5.2 Signal Object Selection

For the final selection of events, some objects are required to pass more stringent requirements, which are described below.

"Signal" jets have a higher threshold of p_{T}>25(30) GeV in the soft(hard)-lepton channels. The signal jets are further required to be associated with the hard-scattering process by demanding that at least 25% of the scalar sum of the p_{T} of all tracks associated with the jet comes from tracks associated with the primary vertex in the event. This requirement is applied in order to remove jets which come from pile-up; it is not applied on jets with a requested p_{T} greater than 30 GeV nor on the b-tagged jets (see below) since the probability of a pile-up jet satisfying either of these requirements is negligible.

Signal jets arising from b-quarks are identified using information about track impact parameters and reconstructed secondary vertices; the b-tagging algorithm MV1 is based on a neural network using the

output weights of IP3D, SV1 and JetFitter+IP3D (defined in [80]) as inputs. While one or two b-jets are requested in the soft single-lepton b-jet channels, the presence of b-jets is vetoed in the soft dimuon channel to remove the $t\bar{t}$ background. In the single-lepton channels, the b-jets are neither requested nor vetoed in the event selection, but are used in the background estimation, as explained in Section 7. The operating point used for the b-tagging is therefore optimized for each channel. In the soft/hard single-lepton and soft single-lepton two b-jet channels, the operating point chosen gives an inclusive b-tagging efficiency of 60% in a simulated sample of $t\bar{t}$ events, while the points chosen in the soft single-lepton one b-jet and soft dimuon channels give inclusive efficiencies of 70% and 80% , respectively. For these operating points with b-jet efficiencies of 60%, 70% and 80%, the algorithm provides rejection factors of approximately 585, 135 and 25 for light quark and gluon jets, respectively, and 8, 5 and 3 for charm jets [81].

The "signal" electrons must pass a higher threshold of 10 (25) GeV in the soft(hard)-lepton channels and are required to be isolated. The isolation requirements depend on the analysis channel, being tighter for channels in which the background coming from misidentified leptons is more important. In the soft-lepton channels, the scalar sum of the p_{T} of tracks within a cone of radius $\Delta R = 0.3$ around the electron (excluding the electron itself) is required to be less than 16% of the electron p_{T}. The distance along the beam direction, $z_0 \sin\theta$, of the electron to the primary vertex must also be ≤ 0.4 mm. Finally, the soft dimuon channel also demands that the significance of the distance of closest approach of the electron to the primary vertex be within three standard deviations in the transverse plane. In the hard-lepton channels, the scalar sum of the p_{T} of tracks within a cone of radius $\Delta R = 0.2$ around the electron (excluding the electron itself) is required to be less than 10% of the electron p_{T}.

Isolation is also required in the "signal" muon definition. In the soft-lepton channels, the scalar sum of the p_{T} of tracks within a cone of radius $\Delta R = 0.3$ around the muon candidate (excluding the muon itself) is required to be less than 12% of the muon p_{T}. The same requirement as in the electron isolation is applied on the distance to the primary vertex along the beam direction and, in the soft dimuon channel, on the significance of the distance of closest approach to the primary vertex in the transverse plane. In the hard-lepton channels, the scalar sum of the p_{T} of tracks within a cone of radius $\Delta R = 0.2$ around the muon candidate (excluding the muon itself) is required to be less than 1.8 GeV.

6 Event Selection

The following variables, derived from the kinematic properties of the reconstructed objects, are used in the event selection.

The minimum distance between the signal lepton (the subleading muon in the soft dimuon channel) and all preselected jets with $|\eta| < 2.5$,

$$\Delta R_{\mathrm{min}} = \min\left(\Delta R(j_1, \ell), \Delta R(j_2, \ell), ..., \Delta R(j_n, \ell)\right),$$

is used to reduce the misidentified lepton background in all soft-lepton signal regions with the exception of the single-lepton 5-jet and the soft single-lepton two b-jet signal regions, as it lowers the signal acceptance in the 5-jet channel and the misidentified-lepton background is small in the two b-jet channel.

The minimal azimuthal angle between the missing transverse momentum and the two leading signal jets,

$$\Delta\phi_{\mathrm{min}} = \min\left(\Delta\phi(\boldsymbol{p}_{\mathrm{T}}^{\mathrm{miss}}, \boldsymbol{p}_{\mathrm{T}}^{\mathrm{jet,1}}), \Delta\phi(\boldsymbol{p}_{\mathrm{T}}^{\mathrm{miss}}, \boldsymbol{p}_{\mathrm{T}}^{\mathrm{jet,2}})\right),$$

is applied to suppress fake $E_{\mathrm{T}}^{\mathrm{miss}}$ background from multijet events in the soft single-lepton two b-jet signal region.

The transverse mass (m_{T}) of the lepton (ℓ) and $\boldsymbol{p}_{\mathrm{T}}^{\mathrm{miss}}$ is defined as

$$m_{\mathrm{T}} = \sqrt{2 p_{\mathrm{T}}^{\ell} E_{\mathrm{T}}^{\mathrm{miss}} (1 - \cos(\Delta\phi(\vec{\ell}, \boldsymbol{p}_{\mathrm{T}}^{\mathrm{miss}})))}.$$

It is used to reject events containing a $W \to \ell\nu$ decay in all signal regions except the soft single-lepton two b-jet signal region where this background is negligible. In the soft dimuon channel, the transverse mass is defined using the subleading muon.

The inclusive effective mass ($m_{\text{eff}}^{\text{inc}}$) is the scalar sum of the p_{T} of the lepton(s), the jets and $E_{\text{T}}^{\text{miss}}$:

$$m_{\text{eff}}^{\text{inc}} = \sum_{i=1}^{\text{N}_\ell} p_{\text{T,i}}^{\ell} + \sum_{j=1}^{\text{N}_{\text{jet}}} p_{\text{T,j}} + E_{\text{T}}^{\text{miss}}$$

where the index i runs over all the signal leptons and the index j runs over all the signal jets in the event. The inclusive effective mass is correlated with the overall mass scale of the hard-scattering and provides good discrimination against SM background, without being too sensitive to the details of the SUSY decay cascade. It is used in the hard single-lepton channels.

The ratio $E_{\text{T}}^{\text{miss}}/m_{\text{eff}}^{\text{inc}}$ is used in the soft single-lepton and soft single-lepton one b-jet signal regions. It is similar to the $E_{\text{T}}^{\text{miss}}$ significance in that it reflects the change in the $E_{\text{T}}^{\text{miss}}$ resolution as a function of the calorimeter activity in the event. In the hard single-lepton channel, a similar ratio is computed, $E_{\text{T}}^{\text{miss}}/m_{\text{eff}}^{\text{excl}}$, where $m_{\text{eff}}^{\text{excl}}$ is the exclusive effective mass, which is defined in a similar way as $m_{\text{eff}}^{\text{inc}}$ with the exception that only the three leading signal jets are considered. This variable is used to remove events with large fake $E_{\text{T}}^{\text{miss}}$ coming from a missing object in the reconstruction.

The contransverse mass [82], m_{CT}, of two b-jets is defined as:

$$m_{\text{CT}}^2\,(b\text{-jet}_1, b\text{-jet}_2) = \left[E_{\text{T}}\,(b\text{-jet}_1) + E_{\text{T}}\,(b\text{-jet}_2)\right]^2 - \left[\boldsymbol{p}_{\text{T}}\,(b\text{-jet}_1) - \boldsymbol{p}_{\text{T}}\,(b\text{-jet}_2)\right]^2,$$

where $E_{\text{T}} = \sqrt{p_{\text{T}}^2 + m^2}$. In this analysis, the boost-corrected contransverse mass [83] is employed, which corrects m_{CT} to account for boosts in the transverse plane due to initial state radiation (ISR) that breaks the invariance of the quantity. This variable is used in the soft single-lepton two b-jet signal region as it gives a measure of the masses of pair-produced heavy particles decaying to final states involving missing transverse momentum.

The dimuon mass, $m_{\mu\mu}$, is required to be outside the Z mass window in the soft dimuon channel in order to reject background events in which a real Z is decaying into muons.

Finally, $H_{\text{T,2}}$ is the scalar sum of the p_{T} of all signal jets excluding the two leading jets. Placing an upper cut on $H_{\text{T,2}}$ in order to suppress further hadronic activity in the event is useful to remove the $t\bar{t}$ background in the low-mass soft single-lepton two b-jet signal region.

This analysis is based on nineteen signal regions, each designed to maximize the sensitivity to different SUSY topologies, as already introduced in Section 5. The selection criteria used to define the various signal regions combined in this analysis are summarized in Table 2 for the signal regions targeting top squark pair production, in Table 3 for the other soft-lepton signal regions and in Table 4 for the hard single-lepton signal regions.

The soft single-lepton signal regions requiring one or two b-jets are designed to cover top squark pair production for which the mass difference between the top squark and the LSP is small and moderate, respectively. A further subdvision is made by varying the requirement on the $E_{\text{T}}^{\text{miss}}$ and, in the soft single-lepton two b-jet case, on m_{CT} and $H_{\text{T,2}}$, in order to cover low-mass or high-mass top squarks. The soft and hard single-lepton signal regions are designed to cover first and second generation squark or gluino pair production, with lower (higher) jet multiplicities for squark (gluino) pair production. The soft-lepton channels focus on compressed scenarios. The soft dimuon signal region is optimized for mUED searches.

In order to have signal regions which are orthogonal to each other in lepton multiplicity and orthogonal to the multilepton analysis [84], a veto is placed on the presence of a second lepton (in the single-lepton channels) or of a third lepton (in the soft dimuon case). In the hard single-lepton channels,

two sets of requirements are optimized for each jet multiplicity: one inclusive signal region optimized for the discovery reach which can also be used to place model-independent limits, and one signal region which is binned in $m_{\text{eff}}^{\text{incl}}$ or $E_{\text{T}}^{\text{miss}}$ (see Section 10) in order to exploit the expected signal shape when placing model-dependent limits. The latter signal regions are made orthogonal in jet multiplicity from one another to allow their statistical combination and have more fine-grained $E_{\text{T}}^{\text{miss}}$, m_{T} and $m_{\text{eff}}^{\text{inc}}$ requirements than in a single overall signal region. As already mentioned in Section 4, the hard single-lepton searches treat the electron and the muon channels independently in the fitting procedure described in Section 9, while they are summed in the soft-lepton channels.

	soft single-lepton one b-jet		**soft single-lepton two b-jets**	
	low-mass	**high-mass**	**low-mass**	**high-mass**
N_ℓ	1 (electron or muon)			
p_{T}^{ℓ}(GeV)	[10,25] (electron) , [6,25] (muon)			
$p_{\text{T}}^{\text{add. }\ell}$ (GeV)	< 7 (electron), < 6 (muon)			
N_{jet}	≥ 3		≥ 2	
$p_{\text{T}}^{\text{jets}}$(GeV)	$> 180,40,40$	$> 180,25,25$	$> 60,60$	
$p_{\text{T}}^{\text{add. jets}}$(GeV)	–		< 50	
$N_{b-\text{tag}}$	≥ 1, but not the leading jet		2	
$E_{\text{T}}^{\text{miss}}$ (GeV)	>250	>300	>200	>300
m_{T} (GeV)	> 100		–	
$E_{\text{T}}^{\text{miss}}/m_{\text{eff}}^{\text{incl}}$	> 0.35		–	
$\Delta R_{\text{min}}(\text{jet}, \ell)$	> 1.0		–	
$\Delta\phi_{\text{min}}$	–		> 0.4	
m_{CT} (GeV)	–		>150	>200
$H_{\text{T},2}$ (GeV)	–		<50	–

Table 2: Overview of the selection criteria for the signal regions targeting top squark pair production. The soft single-lepton one (two) b-jet signal region is designed to cover top squark pair production for which the mass difference between the top squark and the LSP is small (moderate). A further subdvision is made to cover low and high top squark mass hypotheses. As is indicated, the soft leptons are required to have $p_{\text{T}} < 25$ GeV.

	soft single-lepton		soft dimuon
	3-jet	**5-jet**	**2-jet**
N_ℓ	1 (electron or muon)		2 (muons)
p_{T}^{ℓ}(GeV)	[10,25] (electron) , [6,25] (muon)		[6,25]
$p_{\mathrm{T}}^{\text{add. }\ell}$ (GeV)	< 7 (electron), < 6 (muon)		
$m_{\mu\mu}$ (GeV)	–	–	>15 and $\lvert m_{\mu\mu} - m_Z \rvert > 10$
N_{jet}	[3,4]	≥ 5	≥ 2
$p_{\mathrm{T}}^{\text{leading jet}}$(GeV)	> 180		>70
$p_{\mathrm{T}}^{\text{subleading jets}}$(GeV)	> 25		
$N_{b-\text{tag}}$	–	–	0
$E_{\mathrm{T}}^{\text{miss}}$ (GeV)	>400	>300	>170
m_{T} (GeV)	> 100		> 80
$E_{\mathrm{T}}^{\text{miss}}/m_{\text{eff}}^{\text{incl}}$	> 0.3		–
$\Delta R_{\text{min}}(\text{jet}, \ell)$	> 1.0	–	> 1.0

Table 3: Overview of the selection criteria for the soft single-lepton signal regions aimed at covering first and second generation squark or gluino pair production in a compressed scenario and for the soft dimuon signal region designed for the mUED searches. As is indicated, the soft leptons are required to have $p_{\mathrm{T}} < 25$ GeV.

	inclusive (binned) hard single-lepton		
	3-jet	**5-jet**	**6-jet**
N_ℓ	1 (electron or muon)		
p_{T}^{ℓ}(GeV)	> 25		
$p_{\mathrm{T}}^{\text{add. }\ell}$ (GeV)	< 10		
N_{jet}	≥ 3	≥ 5	≥ 6
$p_{\mathrm{T}}^{\text{jet}}$(GeV)	$> 80, 80, 30$	$> 80, 50, 40, 40, 40$	$> 80, 50, 40, 40, 40, 40$
$p_{\mathrm{T}}^{\text{add. jets}}$(GeV)	– (< 40)	– (< 40)	–
$E_{\mathrm{T}}^{\text{miss}}$ (GeV)	>500 (300)	>300	>350 (250)
m_{T} (GeV)	> 150	> 200 (150)	> 150
$E_{\mathrm{T}}^{\text{miss}}/m_{\text{eff}}^{\text{excl}}$	> 0.3	–	–
$m_{\text{eff}}^{\text{incl}}$ (GeV)	> 1400 (800)		> 600

Table 4: Overview of the selection criteria for the hard single-lepton signal regions aimed at covering first and second generation squark or gluino pair production. As is indicated, the hard leptons are required to have $p_{\mathrm{T}} > 25$ GeV. Two sets of requirements are defined for each jet multiplicity: an inclusive signal region and a binned one (see the text). The requirements of the binned signal region are shown in parentheses when they differ from those of the inclusive signal region. Furthermore, the electron and the muon channels are treated independently in the hard single-lepton signal regions.

7 Background Estimation

7.1 $t\bar{t}$ and W+jets Backgrounds

The main sources of SM background in the signal regions are $t\bar{t}$ and W+jets events, in which there is at least one genuine lepton originating from a W decay. These backgrounds are estimated using control regions defined so as to be enriched in SM events from the process of interest while having a low contribution from the signal of interest. The normalization of the simulation is adjusted per analysis channel simultaneously in all its control regions using a fit described in Section 9, and the simulation is used to extrapolate the results to the signal region.

As indicated in Tables 5 and 6, the control regions for the soft single-lepton one and two b-jet signal regions are built by requiring the lepton to have $p_{\mathrm{T}} > 25$ GeV. The $E_{\mathrm{T}}^{\mathrm{miss}}/m_{\mathrm{eff}}^{\mathrm{incl}}$ requirement is also dropped in all control regions for the soft single-lepton one b-jet channels. For each of these signal regions, a $t\bar{t}$ enriched control region is obtained by loosening the requirement on $E_{\mathrm{T}}^{\mathrm{miss}}$ with respect to the signal region. For the W+jets background, the control region is defined by vetoing on the presence of b-jets; in the soft single-lepton one b-jet channels, a lower m_{T} requirement with respect to the signal region is also applied.

Table 7 summarizes the requirements for the soft single-lepton and soft dimuon channels. The soft single-lepton control regions are built using events with lower $E_{\mathrm{T}}^{\mathrm{miss}}$ and m_{T} values than in their respective signal regions and by dropping the requirement on $E_{\mathrm{T}}^{\mathrm{miss}}/m_{\mathrm{eff}}^{\mathrm{incl}}$. The W+jets and $t\bar{t}$ components of these control regions are separated by a requirement on the number of signal jets which are b-tagged. If at least one signal jet is b-tagged, then this event enters the $t\bar{t}$ control region. Otherwise, it is identified as being part of the W+jets control region. In the soft dimuon analysis, the $t\bar{t}$ control region is built by requiring the leading muon to have $p_{\mathrm{T}} >25$ GeV and the subleading one, $p_{\mathrm{T}} > 6$ GeV. The veto on b-tagged jets is reversed to require at least one b-tagged signal jet and the events are required to have lower m_{T} values than in the signal region.

Finally, Table 8 lists the control region requirements for the hard single-lepton channels. They are defined by lowering the requirements on $E_{\mathrm{T}}^{\mathrm{miss}}$ and m_{T} and by dropping the $E_{\mathrm{T}}^{\mathrm{miss}}/m_{\mathrm{eff}}^{\mathrm{excl}}$ requirement in the 3-jet region. The different regions are kept orthogonal by vetoing on the presence of additional jets in each control region. The p_{T} requirements on subleading jets are also lowered with respect to the signal regions to increase the statistics in the control regions. Finally, the W+jets and $t\bar{t}$ components of these control regions are separated by a requirement on the number of signal jets which are b-tagged, considering the first three leading jets. In order to enhance the W+jets contribution over the $t\bar{t}$ contribution in the 6-jet W+jets control region, the m_{T} and $E_{\mathrm{T}}^{\mathrm{miss}}$ requirements are lowered in this region with respect to the 6-jet $t\bar{t}$ control region.

Figure 1 shows the distribution of $E_{\mathrm{T}}^{\mathrm{miss}}/m_{\mathrm{eff}}^{\mathrm{incl}}$ for the $t\bar{t}$ and W+jets control regions of the soft single-lepton one b-jet channel, while Figure 2 shows m_{CT} for similar regions of the soft single-lepton two b-jet channel. Figures 3 and 4 show the $E_{\mathrm{T}}^{\mathrm{miss}}$ and m_{T} distributions in the soft single-lepton and soft dimuon control regions, respectively, while Figures 5 and 6 show the $E_{\mathrm{T}}^{\mathrm{miss}}$ distribution in the hard single-lepton control regions, where the electron and muon channels have been merged for simplicity. Note that all these distributions are shown after the fitting procedure is applied to adjust their normalization, as described in Section 9. As can be seen from these figures, there is reasonable agreement between the data and this Standard Model background estimation within the experimental systematic uncertainties.

	soft single-lepton one b-jet			
	low-mass	**high-mass**	**low-mass**	**high-mass**
	$t\bar{t}$		W + jets	
N_ℓ	1 (electron or muon)			
p_{T}^{ℓ}(GeV)	>25			
$p_{\mathrm{T}}^{\text{add. }\ell}$ (GeV)	< 7 (electron), < 6 (muon)			
N_{jet}	≥ 3			
$p_{\mathrm{T}}^{\text{jets}}$(GeV)	> 180,40,40	> 180,25,25	> 180,40,40	> 180,25,25
$N_{b-\text{tag}}$	≥ 1, but not the leading jet		0	
$E_{\mathrm{T}}^{\text{miss}}$ (GeV)	>150		>250	>300
m_{T} (GeV)	> 100		[40,80]	
ΔR_{min}(jet, ℓ)	> 1.0			

Table 5: Overview of the selection criteria for the $t\bar{t}$ and W + jets control regions used in the search channels requiring one b-jet.

	soft single-lepton two b-jet			
	low-mass	**high-mass**	**low-mass**	**high-mass**
	$t\bar{t}$		W + jets	
N_ℓ	1 (electron or muon)			
p_{T}^{ℓ}(GeV)	>25			
$p_{\mathrm{T}}^{\text{add. }\ell}$ (GeV)	< 7 (electron), < 6 (muon)			
N_{jet}	≥ 2			
$p_{\mathrm{T}}^{\text{jets}}$(GeV)	> 60			
$p_{\mathrm{T}}^{\text{add. jets}}$(GeV)	< 50			
$N_{b-\text{tag}}$	2		0	
$E_{\mathrm{T}}^{\text{miss}}$ (GeV)	>150		>200	>300
$\Delta\phi_{\text{min}}$	> 0.4			
m_{CT} (GeV)	> 150	> 200	>150	>200
$H_{\mathrm{T},2}$ (GeV)	<50	–	<50	–

Table 6: Overview of the selection criteria for the $t\bar{t}$ and W + jets control regions used in the search channels requiring soft single-lepton two b-jets.

	soft single-lepton		soft dimuon
	3-jet	**5-jet**	**2-jet**
	***W*+jets / $t\bar{t}$**		$t\bar{t}$
N_ℓ	1 (electron or muon)		2 (muons)
p_{T}^{ℓ}(GeV)	[10,25] (electron) , [6,25] (muon)		>25,6
$p_{\mathrm{T}}^{\text{add. }\ell}$ (GeV)	< 7 (electron), < 6 (muon)		
$m_{\mu\mu}$ (GeV)	–	–	>15 and $\lvert m_{\mu\mu} - m_Z \rvert > 10$
N_{jet}	[3,4]	≥ 5	≥ 2
$p_{\mathrm{T}}^{\text{leading jet}}$(GeV)	> 180		>70
$p_{\mathrm{T}}^{\text{subleading jets}}$(GeV)	> 25		
$N_{b-\text{tag}}$	0 / ≥ 1		≥ 1
$E_{\mathrm{T}}^{\text{miss}}$ (GeV)	[180,250]		> 170
m_{T} (GeV)	[40,80]		< 80
ΔR_{min}(jet, ℓ)	> 1.0	–	> 1.0

Table 7: Overview of the selection criteria for the *W*+jets and $t\bar{t}$ control regions used in the search channels requiring at least one soft lepton.

	hard single-lepton		
	3-jet	**5-jet**	**6-jet**
	***W*+jets / $t\bar{t}$**		
N_ℓ	1 (electron or muon)		
p_{T}^{ℓ}(GeV)	> 25		
$p_{\mathrm{T}}^{\text{add. }\ell}$ (GeV)	< 10		
N_{jet}	≥ 3	≥ 5	≥ 6
$p_{\mathrm{T}}^{\text{jet}}$(GeV)	> 80, 80, 30	> 80, 50, 30, 30, 30	> 80, 50, 30, 30, 30, 30
$p_{\mathrm{T}}^{\text{add. jets}}$(GeV)	< 30	< 30	–
$N_{b-\text{tag}}$	0 / ≥ 1		
$E_{\mathrm{T}}^{\text{miss}}$ (GeV)	[150,300]		[150,250] / [100,200]
m_{T} (GeV)	[80,150]	[60,150]	[40,150] / [40,80]
$m_{\text{eff}}^{\text{incl}}$ (GeV)	> 800		> 600

Table 8: Overview of the selection criteria for the *W*+jets and $t\bar{t}$ control regions used in the search channels requiring one hard lepton. In these regions, the electron and muon channels are treated separately.

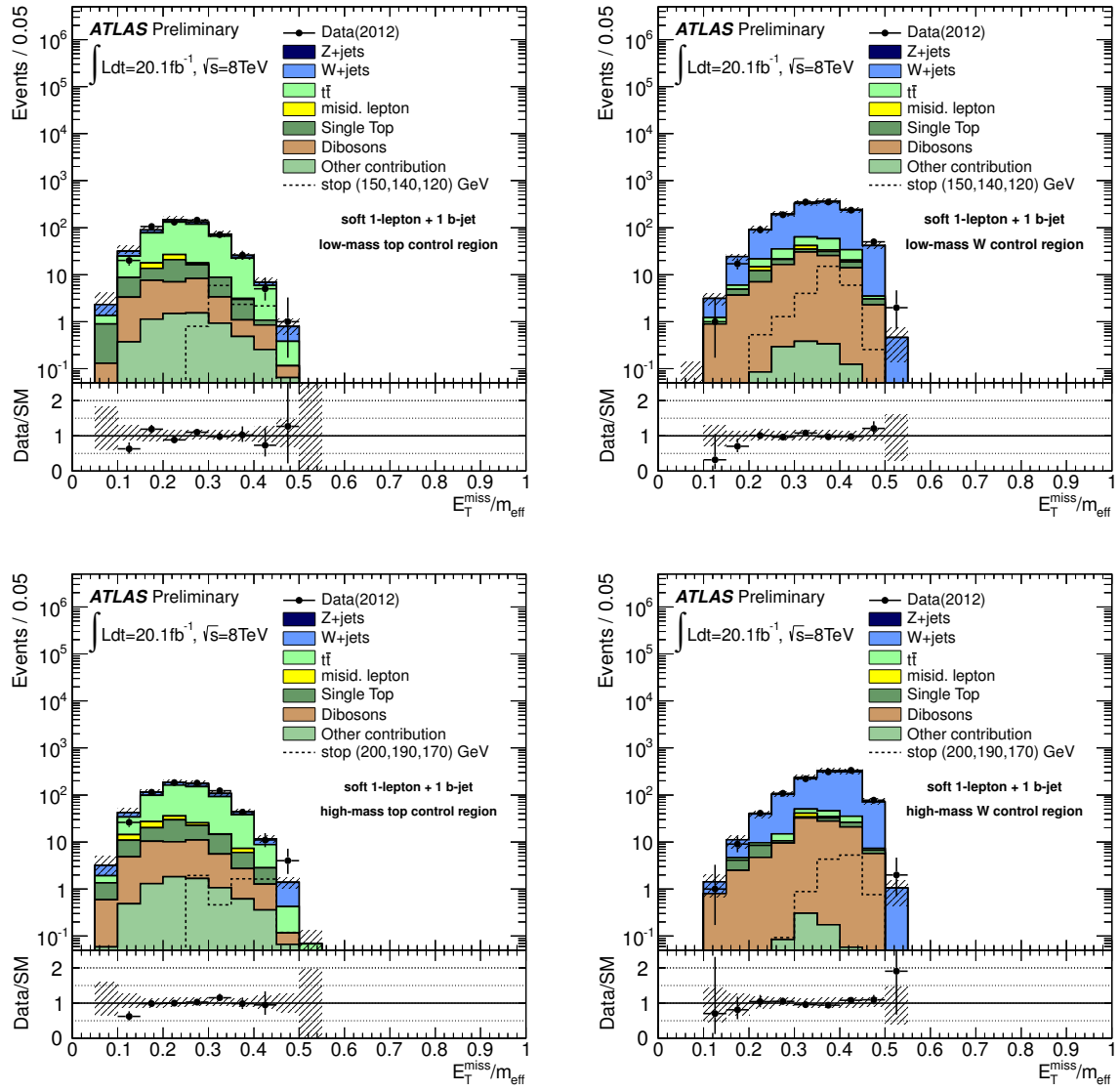

Figure 1: From left to right: $E_{\mathrm{T}}^{\mathrm{miss}}/m_{\mathrm{eff}}^{\mathrm{incl}}$ distribution in the $t\bar{t}$ and W + jets control regions used in the low-mass (top) and high-mass (bottom) soft single-lepton one b-jet channels. The "Data/SM" plots show the ratio between data and the summed Standard Model expectation. The Standard Model expectation is derived from the fit described in Section 9. The uncertainty band on the Standard Model expectation shown here combines the statistical uncertainty on the simulated event samples with the systematic uncertainties on the jet energy scale and resolution, on the lepton identification, momentum/energy scale and resolution, on the $E_{\mathrm{T}}^{\mathrm{miss}}$ calculation, on the b-tagging, and on the data-driven misidentified-lepton background. For illustration, the expected signal distributions are shown for the top squark pair production simplified model with $m_{\tilde{t}}$=150 GeV, $m_{\tilde{\chi}_1^\pm}$=140 GeV and $m_{\tilde{\chi}_1^0}$=120 GeV (in the low-mass channel) and $m_{\tilde{t}}$=200 GeV, $m_{\tilde{\chi}_1^\pm}$=190 GeV and $m_{\tilde{\chi}_1^0}$=170 GeV (in the high-mass channel).

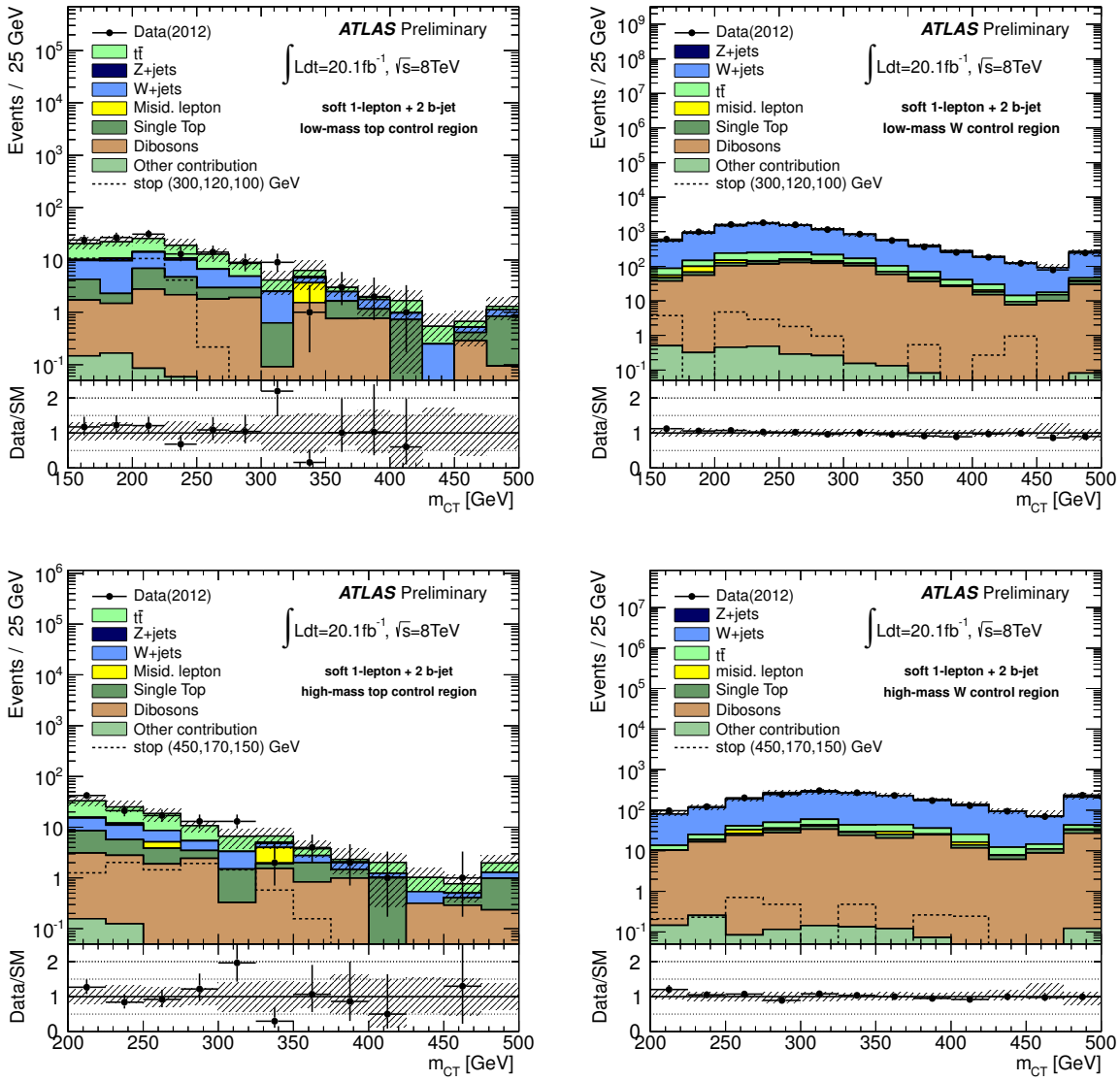

Figure 2: From left to right: m_{CT} distribution in the $t\bar{t}$ and W + jets jets control regions used in the low-mass (top) and high-mass (bottom) soft single-lepton two b-jet channels. The "Data/SM" plots show the ratio between data and the summed Standard Model expectation. The Standard Model expectation is derived from the fit described in Section 9. The uncertainty band on the Standard Model expectation shown here combines the statistical uncertainty on the simulated event samples with the systematic uncertainties on the jet energy scale and resolution, on the lepton identification, momentum/energy scale and resolution, on the $E_{\mathrm{T}}^{\mathrm{miss}}$ calculation, on the b-tagging, and on the data-driven misidentified-lepton background. The last bin includes the overflow. For illustration, the expected signal distributions are shown for the top squark pair production simplified model with $m_{\tilde{t}}$=300 GeV, $m_{\tilde{\chi}_1^{\pm}}$=120 GeV and $m_{\tilde{\chi}_1^0}$=100 GeV (in the low-mass channel) and $m_{\tilde{t}}$=450 GeV, $m_{\tilde{\chi}_1^{\pm}}$=170 GeV and $m_{\tilde{\chi}_1^0}$=150 GeV (in the high-mass channel).

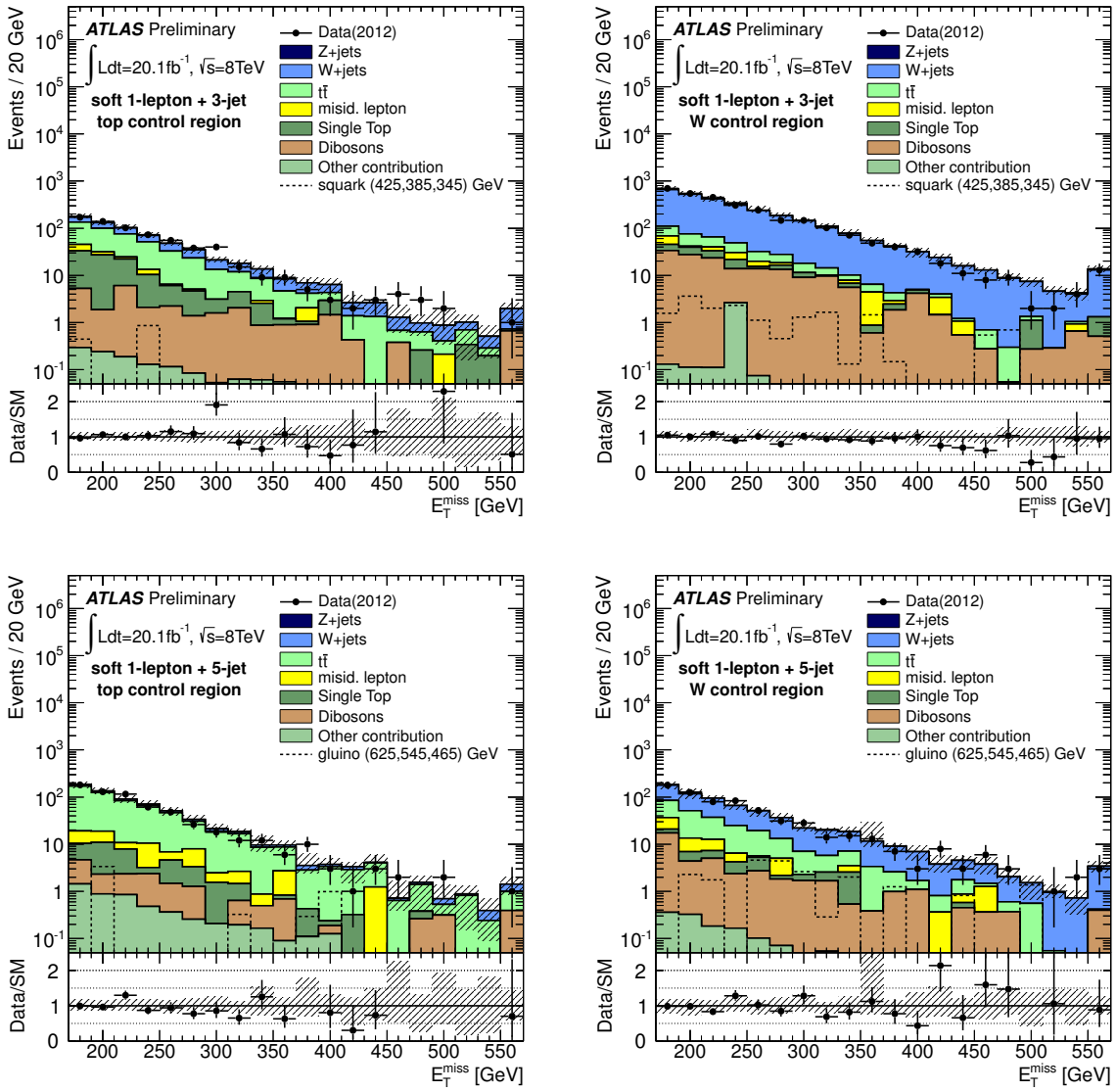

Figure 3: $E_{\mathrm{T}}^{\mathrm{miss}}$ distribution in the 3-jet (top) and 5-jet (bottom) $t\bar{t}$ (left) and W+jets (right) control regions, before the upper $E_{\mathrm{T}}^{\mathrm{miss}}$ requirements are applied, used in the soft single-lepton channels. The "Data/SM" plots show the ratio between data and the summed Standard Model expectation. The Standard Model expectation is derived from the fit described in Section 9. The uncertainty band on the Standard Model expectation shown here combines the statistical uncertainty on the simulated event samples with the systematic uncertainties on the jet energy scale and resolution, on the lepton identification, momentum/energy scale and resolution, on the $E_{\mathrm{T}}^{\mathrm{miss}}$ calculation, on the b-tagging, and on the data-driven misidentified-lepton background. The last bin includes the overflow. For illustration, the expected signal distribution is shown for first and second generation squark pair production with $m_{\tilde{q}} = 425$ GeV, $m_{\tilde{\chi}_1^\pm}$=385 GeV and $m_{\tilde{\chi}_1^0} = 345$ GeV in the 3-jet channel, and for gluino pair production with $m_{\tilde{g}} = 625$ GeV, $m_{\tilde{\chi}_1^\pm}$=545 GeV and $m_{\tilde{\chi}_1^0} = 465$ GeV in the 5-jet channel.

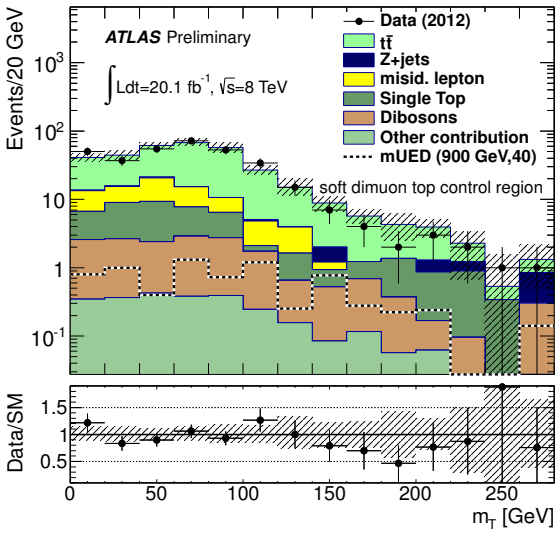

Figure 4: m_{T} distribution in the $t\bar{t}$ control region (before the upper m_{T} requirement is applied) used in the soft dimuon channel. The "Data/SM" plots show the ratio between data and the summed Standard Model expectation. The Standard Model expectation is derived from the fit described in Section 9. The uncertainty band on the Standard Model expectation shown here combines the statistical uncertainty on the simulated event samples with the systematic uncertainties on the jet energy scale and resolution, on the lepton identification, momentum/energy scale and resolution, on the $E_{\mathrm{T}}^{\mathrm{miss}}$ calculation, on the b-tagging, and on the data-driven misidentified-lepton background. The last bin includes the overflow. For illustration, the expected signal distribution of the mUED model point with R = 900 GeV and ΛR=40 is also shown.

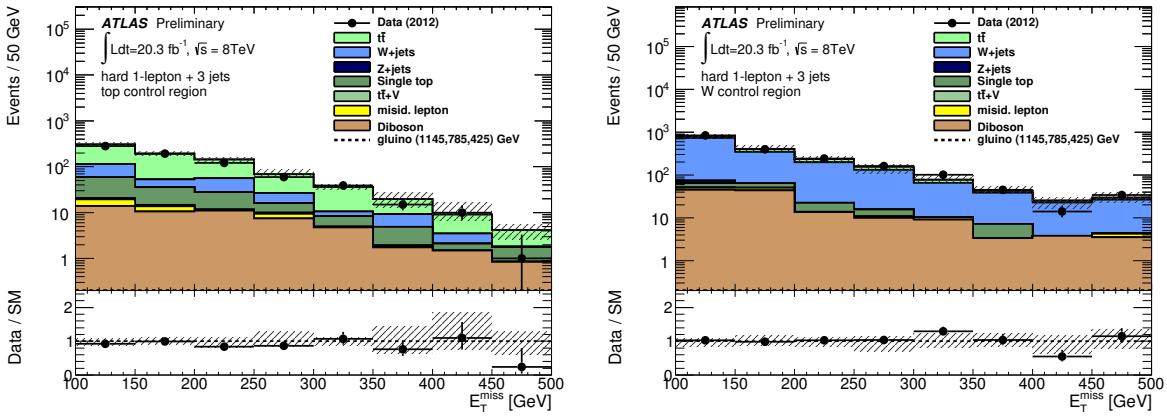

Figure 5: $E_{\mathrm{T}}^{\mathrm{miss}}$ distribution in the 3-jet $t\bar{t}$ (left) and W+jets (right) control regions, before the upper $E_{\mathrm{T}}^{\mathrm{miss}}$ requirements are applied, used in the hard single-electron channels. The "Data/SM" plots show the ratio between data and the summed Standard Model expectation. The Standard Model expectation is derived from the fit described in Section 9. The uncertainty band on the Standard Model expectation shown here combines the statistical uncertainty on the simulated event samples with the systematic uncertainties on the jet energy scale and resolution, on the lepton identification, momentum/energy scale and resolution, on the $E_{\mathrm{T}}^{\mathrm{miss}}$ calculation, on the b-tagging, and on the data-driven misidentified-lepton background. The last bin includes the overflow.

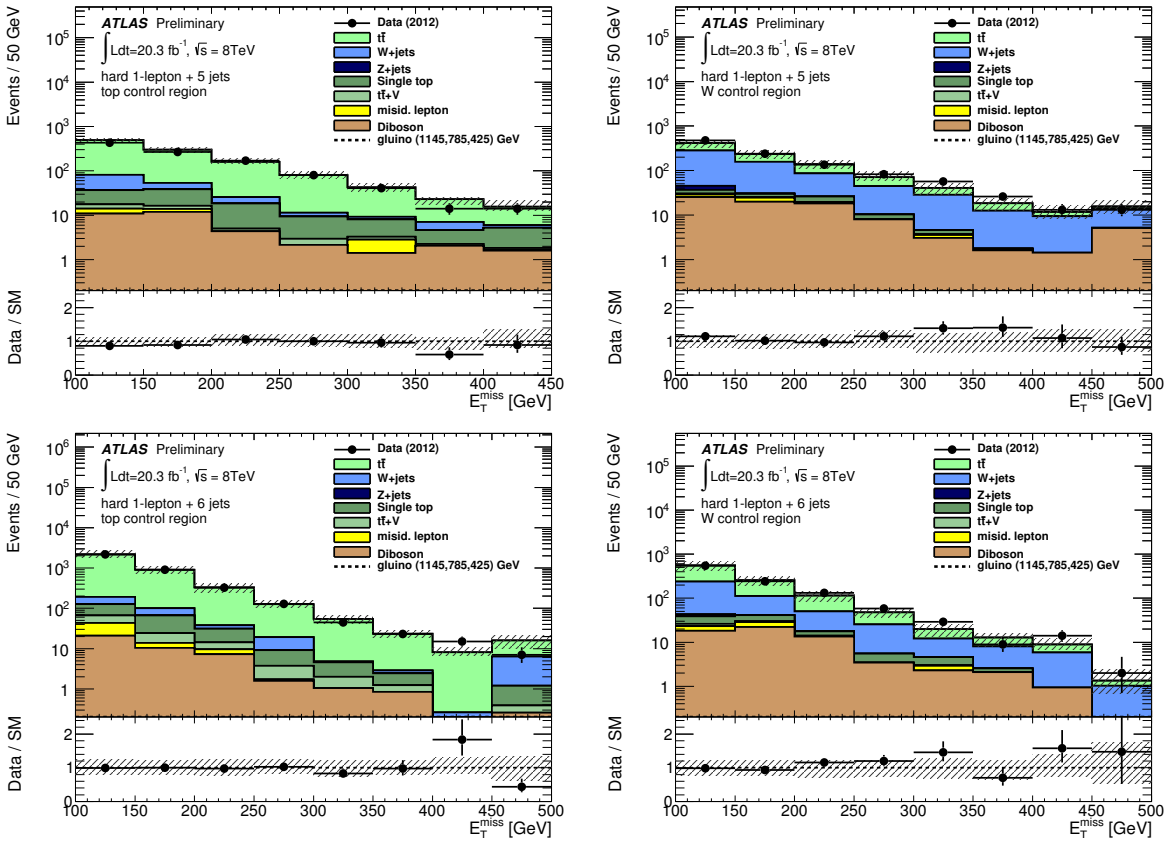

Figure 6: $E_{\mathrm{T}}^{\mathrm{miss}}$ distribution in the 5-jet (top) and 6-jet (bottom) $t\bar{t}$ (left) and W+jets (right) control regions, before the upper $E_{\mathrm{T}}^{\mathrm{miss}}$ requirements are applied, used in the hard single-electron channels. The "Data/SM" plots show the ratio between data and the summed Standard Model expectation. The Standard Model expectation is derived from the fit described in Section 9. The uncertainty band on the Standard Model expectation shown here combines the statistical uncertainty on the simulated event samples with the systematic uncertainties on the jet energy scale and resolution, on the lepton identification, momentum/energy scale and resolution, on the $E_{\mathrm{T}}^{\mathrm{miss}}$ calculation, on the b-tagging, and on the data-driven misidentified-lepton background. The last bin includes the overflow.

7.2 Misidentified-lepton Background

Events with misidentified leptons can also mimic the signal if they have sufficiently large $E_{\mathrm{T}}^{\mathrm{miss}}$. A jet can be misidentified as a lepton, or a real lepton can arise as a decay product of b- or c-hadrons in jets but can still be sufficiently isolated. Such lepton-like objects are collectively referred to as misidentified leptons in this note. The multijet and $Z(\rightarrow \nu\nu)$+jets processes with such misidentified leptons are an important source of misidentified-lepton background in the single-lepton analyses, while $W \rightarrow \ell\nu$+jets and $t\bar{t}$ production (where one of the leptons comes from a W decay and the other is from a b-hadron decay) dominate the misidentified-lepton background in the soft dimuon analysis.

The misidentified-lepton background in the signal region, and in the W+jets and $t\bar{t}$ control regions where it is more significant, is estimated entirely from the data by a matrix method described below. This procedure is applied separately for electrons and muons.

In this method, the process creating the misidentified lepton is enhanced in a control sample with all the signal or control region criteria applied but where preselected leptons are used instead of signal leptons. If N_{pass} and N_{fail} are the number of events found passing or failing the signal lepton selection criteria in this control sample, then the number of events with a misidentified lepton in a single-lepton signal or control region is given by:

$$N_{\mathrm{pass}}^{\mathrm{misid}} = \frac{N_{\mathrm{fail}} - (1/\epsilon^{\mathrm{real}} - 1)N_{\mathrm{pass}}}{1/\epsilon^{\mathrm{misid}} - 1/\epsilon^{\mathrm{real}}}$$

where ϵ^{real} is the identification efficiency for real leptons and $\epsilon^{\mathrm{misid}}$ is the misidentification efficiency for misidentified leptons. For dileptonic signal or control regions, the estimation of this background is based on the same principle, this time using a four-by-four matrix to take into account the different misidentification combinations: the leading lepton, the subleading lepton or both leptons are misidentified, or both leptons are real.

The identification efficiency ϵ^{real} is obtained from data using $Z \rightarrow \ell^+\ell^-$ events. The lepton misidentification efficiency $\epsilon^{\mathrm{misid}}$ is estimated in control regions enriched in multijet events. The multi-jet control region is composed of events containing at least one preselected lepton, at least one signal jet with $p_{\mathrm{T}} > 60$ GeV, $m_{\mathrm{T}} < 40$ GeV and $E_{\mathrm{T}}^{\mathrm{miss}} < 30$ GeV. As the control region is defined at low $E_{\mathrm{T}}^{\mathrm{miss}}$ values, the triggers described in Section 4 cannot be used here. A combination of prescaled single lepton triggers and unprescaled dilepton triggers is used instead. The events are split into two samples depending on whether they have at least one b-tagged jet, in order to allow $\epsilon^{\mathrm{misid}}$ to vary as a function of the misidentified lepton source.

7.3 Other Backgrounds

All other backgrounds are estimated from the simulation, using the most accurate theoretical cross sections available. This includes single-top, dibosons, $t\bar{t} + W$ and $t\bar{t} + Z$ production. They account for at most 20% of the background in all signal regions.

8 Systematic Uncertainties

Systematic uncertainties have an impact on the expected event yields in the control regions and on the extrapolation factors used to derive the background yields in the signal region. The following detector-related systematic uncertainties are taken into account.

The jet energy scale (JES) uncertainty has been measured using a combination of test beam, simulation and in-situ measurements from pp collisions as described in Refs. [72, 73] and depends on p_{T} and η. The jet energy resolution (JER) uncertainty has also been estimated using in-situ measurements [85].

Additional contributions to the JES and JER uncertainties arising from the high luminosity and pile-up in 2012 data are taken into account. Uncertainties on the lepton identification, momentum/energy scale and resolution are estimated from samples of $Z \to \ell^+\ell^-$, $J/\psi \to \ell^+\ell^-$ and $W^\pm \to \ell^\pm\nu$ decays [74,76,77]. These jet and lepton uncertainties are propagated to the $E_{\mathrm{T}}^{\mathrm{miss}}$ calculation which also includes an uncertainty coming from the energy deposits which are not associated to a jet or a lepton [79]. Uncertainties associated with the b-tagging efficiency are derived from data samples of jets containing muons [81] while uncertainties associated to the probability of mistakenly b-tagging a jet which does not originate from a b-quark are determined from inclusive jet samples [86]. An uncertainty (1-5%) is also assigned to the trigger efficiency based on studies comparing the plateau efficiency in data to that obtained with Monte Carlo samples. Uncertainties are also assigned to the misidentified lepton background estimation, including a statistical uncertainty on the number of events in the control samples, an uncertainty on the identification efficiency and an uncertainty on the subtraction of other backgrounds from the control samples used to estimate the misidentification efficiency.

The following theory-related uncertainties are also taken into account. For the W+jets background, an uncertainty due to the factorization and renormalization scales is computed by varying these scales by a factor of two, up and down with respect to the nominal setting. For the ALPGEN W+jets samples, the jet p_{T} threshold used in the MLM matching is also varied from 25 to 40 GeV and the difference is taken as one standard deviation. As only a finite number of partons is generated in the nominal SHERPA samples, an uncertainty is also derived from the comparison of two samples with different numbers of generated partons. An additional uncertainty of 24% is assigned to the heavy flavour component of the SHERPA W+jets background for the b-jet channels [87]. PDF uncertainties are also included.

To estimate the theoretical uncertainties associated to the $t\bar{t}$ background, POWHEG [50] samples are used for which the renormalization and factorization scales are varied by a factor two, up and down with respect to the nominal samples. The uncertainty due to the parton shower modeling is evaluated by comparing the nominal POWHEG+PYTHIA samples to POWHEG+Herwig/Jimmy samples. The PYTHIA parameters controlling the initial and final state radiation are also varied to produce an uncertainty. PDF uncertainties are also included.

For the single top, diboson and $t\bar{t}$+W/Z backgrounds, relative uncertainties of 50%, 50% and 30%, respectively, are assigned to reflect the cross section and modeling uncertainties on these processes.

For the simplified signal models, theoretical uncertainties on the acceptance are also assessed. In particular, the uncertainty on the modeling of initial state radiation plays an important role for small mass differences in the decay cascade. These uncertainties are estimated using MadGraph5+PYTHIA samples for which the following parameters are varied up and down in turn by a factor two: the MadGraph scale used to determine the event-by-event renormalization and factorization scale, the MadGraph parameter used to determine the scale for QCD radiation, the PYTHIA parameter which controls the Λ_{QCD} value used for final state radiation (the upward variation for this parameter uses a factor of 1.5) and the MadGraph parameter used for jet matching. For the mUED sample nominally generated with Herwig++, the same procedure was applied, generating one of the main production diagrams in MadGraph and evaluating its uncertainty related to the MadGraph renormalization and factorization scales as well as the scale for QCD radiation.

9 Background Fit

The background in the signal region is estimated with a fit based on the profile likelihood method [88]. The inputs to the fit are as follows, for each of the search regions:

1. The number of events observed in each of the control regions, and the corresponding number of events expected from simulation. The inputs are shown in Figures 1-6.

2. The transfer factors (obtained from the simulation) which relate the number of predicted W/Z+jets or $t\bar{t}$ events in their associated control region to that predicted in the signal region.

3. The number of misidentified-lepton events in each region obtained with the data-driven method.

4. The number of events predicted by the simulation in each region for the single-top, diboson and $t\bar{t}$+W/Z backgrounds.

The number of events in each of these regions is described using a Poisson probability density function. There are two free parameters considered per channel: an overall normalization scale for the W/Z+jets background and another scale for the $t\bar{t}$ background[1]. The other background sources are allowed to vary in the fit within their respective uncertainties. The statistical and systematic uncertainties (see Section 8) on the expected values are included in the fit as nuisance parameters which are typically constrained by a Gaussian function with a width corresponding to the size of the uncertainty considered; correlations between these parameters are taken into account. The product of the various probability density functions forms the likelihood which the fit maximizes by adjusting the free and nuisance parameters. In the hard-lepton signal regions, the electron and muon channels are treated separately but share common $t\bar{t}$ and W+jets normalization factors for a given jet multiplicity signal region.

The background fit results are cross-checked in validation regions located between, and orthogonal to the control and signal regions. The data in the validation regions are not used to constrain the fits; they are only used to compare the results of the fits to statistically independent observations. The criteria used to define the validation regions are summarized in Tables 9–12. In the b-jet channels (see Tables 9 and 10) validation regions are defined for each of the high-mass and low-mass signal regions. They are used to cross check the extrapolations in lepton p_{T}, m_{T} and $E_{\mathrm{T}}^{\mathrm{miss}}$ between the control and signal regions as well as cross check the W + heavy flavour jets component in the soft single-lepton one b-jet channels. As shown in Table 11, the soft single-lepton channel uses three validation regions to probe the m_{T} and $E_{\mathrm{T}}^{\mathrm{miss}}$ extrapolations of each control region (3-jet or 5-jet, W+jets or $t\bar{t}$ regions); there are therefore twelve validation regions in the soft single-lepton channel. In the soft dimuon case, shown in the same table, three validation regions are defined to cross-check the lepton p_{T} and the m_{T} extrapolations and the b-jet veto. Finally, in the hard single-lepton channels (see Table 12), each signal region is associated to two validation regions in order to probe the $E_{\mathrm{T}}^{\mathrm{miss}}$ and the m_{T} extrapolations independently, treating the electron and muon channels separately.

	soft single-lepton one b-jet					
	low-mass	**high-mass**	**low-mass**	**high-mass**	**low-mass**	**high-mass**
	soft-lepton region		**hard-lepton region**		**W + heavy flavour jets region**	
p_{T}^{ℓ}(GeV)	[10,25] (electron), [6,25] (muon)		> 25			
$N_{b-\mathrm{tag}}$	≥ 1, but not the leading jet					
$E_{\mathrm{T}}^{\mathrm{miss}}$ (GeV)	[150,250]	[150,300]	>250	>300	>150	
m_{T} (GeV)	> 100		[80,100]		[40,80]	
$E_{\mathrm{T}}^{\mathrm{miss}}/m_{\mathrm{eff}}^{\mathrm{incl}}$	> 0.35					

Table 9: Validation region definitions for the soft single-lepton one b-jet channels. Only the variables for which the selection differs from the respective control region are shown.

The comparison of observed versus predicted event counts in the validation regions as obtained from the background-only fit are summarized in Figure 7. Good agreement is seen between the predicted

[1]Note that the fit can introduce a negative correlation between the $t\bar{t}$ and W+jets normalization scales. This negative correlation increases the relative uncertainty on the individual samples, but the sum of the two contributions (in which this negative correlation cancels) is estimated more precisely.

	soft single-lepton two b-jet			
	low-mass	**high-mass**	**low-mass**	**high-mass**
	soft-lepton region		**hard-lepton region**	
p_{T}^{ℓ}(GeV)	[10,25] (electron), [6,25] (muon)		> 25	
$N_{b-\mathrm{tag}}$	2			
$E_{\mathrm{T}}^{\mathrm{miss}}$ (GeV)	[150,200]	[150,300]	>150	

Table 10: Validation region definitions for the soft single-lepton two b-jet channels. Only the variables for which the selection differs from the respective control region are shown.

	soft single-lepton			**soft dimuon**		
	m_{T} **region**	**interm.** $E_{\mathrm{T}}^{\mathrm{miss}}$ **region**	**high** $E_{\mathrm{T}}^{\mathrm{miss}}$ **region**	m_{T} **region**	**low** p_{T} **region**	b**-veto region**
p_{T}^{ℓ}(GeV)	[10,25] (electron), [6,25] (muon)			>25	[6,25]	>25
$N_{b-\mathrm{tag}}$	–			–	–	0
$E_{\mathrm{T}}^{\mathrm{miss}}$ (GeV)	[180,250]	[250,350]	>350	> 170		
m_{T} (GeV)	>80	[40,100]		> 80	< 80	

Table 11: Validation region definitions for the soft single-lepton and the dilepton channels. In the soft single-lepton case, these three validation regions are defined for each of the 3-jet or 5-jet, W+jets or $t\bar{t}$ control regions; there are therefore twelve different validation regions. Only the variables for which the selection differs from the respective control region are shown.

and observed yields in all regions; the largest discrepancy, which is not significant, is seen in the soft single-lepton one b-jet low-mass soft-lepton validation region[2].

The dominant uncertainties in the background prediction are as follows.

The statistical uncertainty of the simulated samples is a dominant uncertainty for all signal regions except the soft single-lepton 5-jet and the soft single-lepton two b-jet low-mass signal regions. For the regions where it is important, it gives a relative uncertainty of 15% on the yield, except in the soft dimuon signal region where it reaches 30% and in the hard single-electron 5-jet signal region for which it reaches 40%. The statistical uncertainty in the simulated samples also limits the accuracy in the determination

	hard single-lepton					
	3-jet		**5-jet**		**6-jet**	
	$E_{\mathrm{T}}^{\mathrm{miss}}$ **region**	m_{T} **region**	$E_{\mathrm{T}}^{\mathrm{miss}}$ **region**	m_{T} **region**	$E_{\mathrm{T}}^{\mathrm{miss}}$ **region**	m_{T} **region**
$p_{\mathrm{T}}^{\mathrm{jet}}$(GeV)	> 80, 80, 30		> 80, 50, 40, 40, 40		> 80, 50, 40, 40, 40, 40	
$p_{\mathrm{T}}^{\mathrm{add.\ jets}}$(GeV)	< 40		< 40		–	
$N_{b-\mathrm{tag}}$	–					
$E_{\mathrm{T}}^{\mathrm{miss}}$ (GeV)	[300,500]	[150,300]	[300,500]	[150,300]	[250,500]	[150,250]
m_{T} (GeV)	[60,150]	[150,320]	[60,150]	[150,320]	[60,150]	[120,320]

Table 12: Validation region definitions for the hard single-lepton channels. The electron and muon channels are treated independently. Only the variables for which the selection differs from the respective control region are shown.

[2]Note that the measure used in the figure is not identical to the procedure used here to quantify the discovery significance of an excess (see [88] for a description of this procedure). In particular, for a low number of events, the measure used in the figure overestimates the discovery significance.

of several of the other systematic uncertainties mentioned below.

The uncertainties related to the $t\bar{t}$ background parton shower modeling is an important uncertainty for the soft single-lepton, the hard single-lepton 6-jet, the soft dimuon and the soft single-lepton two b-jet high-mass signal regions. In these regions, this uncertainty is on the order of 10-20%, except for the soft dimuon channel for which it reaches 50%. The uncertainties related to the $t\bar{t}$ factorization scale is at the 10% level for the hard single-lepton 5-jet signal region, while the uncertainty on the $t\bar{t}$ yield is at the 10-20% level for the hard single-lepton 3-jet and the soft single-lepton two b-jet signal regions.

The JES and JER uncertainty amounts to 10-15% for the soft single-lepton 3-jet and soft single-lepton one b-jet high-mass signal regions. The b-tagging uncertainty reaches 20% for the soft single-lepton two b-jet high-mass and soft dimuon signal regions. The uncertainty related to the misidentified lepton background is at the 10 % level for the soft single-lepton one b-jet high-mass and the hard single-muon 6-jet signal regions. The lepton efficiency (at approximately 20%) is important for the soft single-lepton two b-jet high-mass signal region. Finally, the uncertainty related to the $W+b\bar{b}$ component of the W+jets background is approximately 10% for the soft single-lepton two b-jet low-mass signal region.

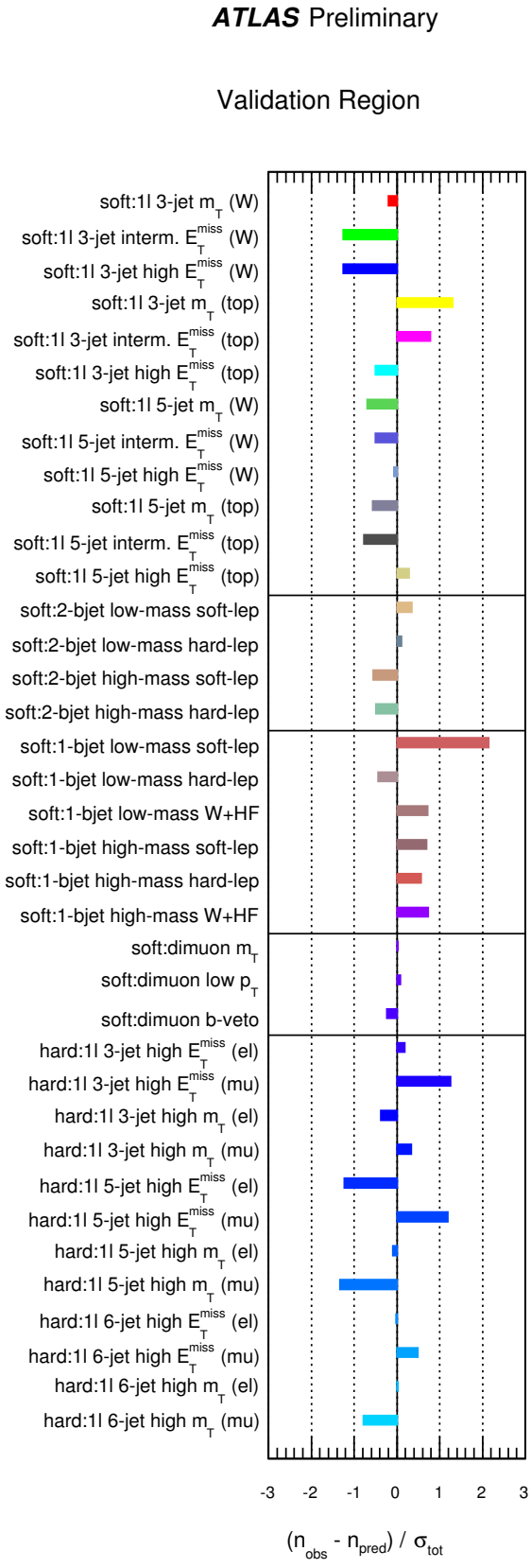

Figure 7: Summary of the fit results: for each validation region (see Tables 9-12), the difference between the observed and predicted number of events, divided by the total (statistical and systematic) uncertainty on the prediction, is shown.

	soft single-lepton one b-jet		soft single-lepton two b-jet	
	low-mass	high-mass	low-mass	high-mass
Observed	8	6	24	3
Fitted background	6.1 ± 1.4	4.0 ± 1.1	24.1 ± 4.1	3.6 ± 1.4
Fitted $t\bar{t}$ events	4.0 ± 1.1	2.3 ± 0.7	9.4 ± 4.5	1.6 ± 1.0
Fitted single-top events	0.8 ± 0.6	0.3 ± 0.2	1.5 ± 0.8	$0.3^{+0.4}_{-0.3}$
Fitted W+jets events	0.6 ± 0.2	0.5 ± 0.3	8.8 ± 3.1	1.1 ± 0.5
Fitted misidentified lepton events	$0.4^{+0.5}_{-0.4}$	$0.4^{+0.5}_{-0.4}$	2.5 ± 1.9	$0.00^{+0.03}_{-0.00}$
Fitted other background events	0.4 ± 0.2	0.4 ± 0.2	1.9 ± 0.9	0.6 ± 0.4
MC expected SM events	7.1 ± 1.7	4.8 ± 1.3	24.7 ± 5.0	3.9 ± 1.6
MC expected $t\bar{t}$ events	4.8 ± 1.3	2.9 ± 0.9	8.4 ± 2.0	1.5 ± 0.8
MC expexted single-top events	0.8 ± 0.6	0.3 ± 0.2	1.5 ± 0.8	$0.3^{+0.4}_{-0.3}$
MC expected W+jets events	0.8 ± 0.3	0.7 ± 0.4	10.4 ± 3.4	1.6 ± 0.6
Data-driven misidentified lepton events	$0.4^{+0.5}_{-0.4}$	$0.4^{+0.5}_{-0.4}$	2.5 ± 1.9	$0.00^{+0.03}_{-0.00}$
MC expected other background events	0.4 ± 0.2	0.4 ± 0.2	2.0 ± 0.9	0.6 ± 0.4

Table 13: Background fit results for the soft single-lepton one and two b-jet signal regions, for an integrated luminosity of 20.1 fb^{-1}. Nominal MC expectations (normalized to MC cross-sections) are given for comparison. The uncertainties shown here combine the statistical uncertainty on the simulated event samples with the systematic uncertainties.

10 Results and Interpretation

The distributions of $E_{\mathrm{T}}^{\mathrm{miss}}$ in the soft single-lepton one b-jet and the soft single-lepton signal regions, of m_{T} in the soft dimuon signal region, of m_{CT} in the soft single-lepton two b-jet signal regions, and of $m_{\mathrm{eff}}^{\mathrm{incl}}$ ($E_{\mathrm{T}}^{\mathrm{miss}}$) in the binned hard single-lepton 3-jet and 5-jet (6-jet) signal regions are shown in Figures 8–11, respectively.

The results of the fit in the different signal regions are shown in Tables 13–16: the number of events seen in the 19 signal regions presented in these tables is consistent with the Standard Model expectations. The largest discrepancy occurs in the soft dimuon channel where 7 events are observed when 1.6 ± 1.0 events are expected. This results in a p-value for the background-only hypothesis of 0.01 (2.3σ).

Limits on the visible cross section of a beyond the Standard Model contribution, defined by production cross section times acceptance times efficiency, are derived from the numbers presented in Tables 13–16. Limits on the number of non-SM events in the signal region, derived using the CL_s prescription [89], are divided by the integrated luminosity to obtain the limits on the visible cross section. The limits at 95% confidence level (CL) are shown in Table 17. For the hard-lepton channels, the limits are shown both for the binned and inclusive signal regions, treating the electron and muon channels independently. One can see that the inclusive signal regions place more stringent limits on the visible cross section than the binned signal regions. This is expected as these signal regions have tighter requirements and as the binning in $m_{\mathrm{eff}}^{\mathrm{incl}}$ or $E_{\mathrm{T}}^{\mathrm{miss}}$ is not exploited here. As explained in Section 6, the binned signal regions are interesting when placing limits on specific models, using their shape in $m_{\mathrm{eff}}^{\mathrm{incl}}$ or $E_{\mathrm{T}}^{\mathrm{miss}}$ to enhance the discriminating power of the search as will be done later in this Section.

	soft single-lepton		soft dimuon
	3-jet	5-jet	2-jet
Observed events	7	9	7
Fitted background events	5.6 ± 1.6	14.8 ± 3.7	1.6 ± 1.0
Fitted $t\bar{t}$ events	1.3 ± 1.0	7.8 ± 3.3	1.2 ± 1.0
Fitted W+jets events	2.6 ± 0.7	2.1 ± 0.9	-
Fitted diboson events	0.6 ± 0.4	0.7 ± 0.4	0.4 ± 0.3
Fitted misidentified lepton events	$0.00^{+0.05}_{-0.00}$	3.3 ± 1.4	$0.0^{+0.3}_{-0.0}$
Fitted other background events	1.1 ± 0.5	0.9 ± 0.5	$0.01^{+0.06}_{-0.01}$
MC expected SM events	6.3 ± 1.9	15.9 ± 3.8	1.9 ± 1.2
MC expected $t\bar{t}$ events	1.4 ± 1.1	7.8 ± 3.0	1.5 ± 1.2
MC expected W+jets events	3.1 ± 0.9	3.2 ± 0.9	-
MC expected diboson events	0.6 ± 0.4	0.7 ± 0.4	0.4 ± 0.3
data-driven misidentified lepton events	$0.00^{+0.05}_{-0.00}$	3.3 ± 1.4	$0.0^{+0.3}_{-0.0}$
MC expected other background events	1.1 ± 0.6	0.9 ± 0.4	$0.01^{+0.06}_{-0.01}$

Table 14: Background fit results for the soft single-lepton and soft dimuon signal regions, for an integrated luminosity of 20.1 fb^{-1}. Nominal MC expectations (normalized to MC cross-sections) are given for comparison. Note that the W+jets component for the soft dimuon channel is included in the misidentified lepton background. The uncertainties shown here combine the statistical uncertainty on the simulated event samples with the systematic uncertainties.

	binned hard single-lepton					
	3-jet		5-jet		6-jet	
	electron	muon	electron	muon	electron	muon
Observed events	45	28	12	7	7	7
Fitted background events	46.4 ± 8.0	38.1 ± 5.8	12.2 ± 5.2	7.1 ± 1.6	9.7 ± 2.0	7.4 ± 1.7
Fitted $t\bar{t}$ events	23.8 ± 6.4	20.0 ± 5.0	7.4 ± 3.3	5.6 ± 1.5	8.0 ± 1.9	5.6 ± 1.5
Fitted W+jets events	15.4 ± 5.5	10.7 ± 4.0	3.1 ± 2.2	0.4 ± 0.4	$0.1^{+0.2}_{-0.1}$	0.3 ± 0.3
Fitted diboson events	4.4 ± 2.3	3.3 ± 1.7	0.9 ± 0.6	0.4 ± 0.2	0.5 ± 0.3	0.06 ± 0.03
Fitted misidentified lepton events	$0.4^{+0.5}_{-0.4}$	$0.8^{+0.9}_{-0.8}$	$0.01^{+0.08}_{-0.01}$	$0.0^{+0.03}_{-0.0}$	$0.07^{+0.09}_{-0.07}$	$0.8^{+0.9}_{-0.8}$
Fitted other background events	2.3 ± 0.8	3.3 ± 1.1	0.7 ± 0.3	0.6 ± 0.2	1.0 ± 0.3	0.6 ± 0.1
MC expected SM events	54.8 ± 10.3	43.0 ± 7.1	14.1 ± 6.3	7.0 ± 1.6	10.1 ± 1.9	7.9 ± 1.7
MC expected $t\bar{t}$ events	23.3 ± 3.7	19.7 ± 2.6	7.1 ± 3.0	5.3 ± 1.2	8.4 ± 1.7	6.0 ± 1.3
MC expected W+jets events	24.4 ± 7.3	16.1 ± 5.1	5.3 ± 3.4	0.6 ± 0.5	0.2 ± 0.2	0.5 ± 0.5
MC expected diboson events	4.5 ± 2.3	3.4 ± 1.7	0.9 ± 0.6	0.4 ± 0.2	0.6 ± 0.3	0.07 ± 0.03
data-driven misidentified lepton events	$0.4^{+0.5}_{-0.4}$	$0.8^{+0.9}_{-0.8}$	$0.01^{+0.08}_{-0.01}$	$0.0^{+0.03}_{-0.0}$	$0.07^{+0.09}_{-0.07}$	$0.8^{+0.9}_{-0.8}$
MC expected other background events	2.1 ± 0.8	3.1 ± 1.2	0.8 ± 0.3	0.7 ± 0.2	1.0 ± 0.3	0.6 ± 0.2

Table 15: Background fit results for the binned hard single-lepton signal regions, for an integrated luminosity of 20.3 fb^{-1}. Nominal MC expectations (normalized to MC cross-sections) are given for comparison. The uncertainties shown here combine the statistical uncertainty on the simulated event samples with the systematic uncertainties.

	inclusive hard single-lepton					
	3-jet		5-jet		6-jet	
	electron	muon	electron	muon	electron	muon
Observed events	4	5	4	2	2	0
Fitted background events	3.9 ± 1.0	2.7 ± 0.9	3.6 ± 1.0	2.5 ± 0.8	2.0 ± 0.7	1.7 ± 0.6
Fitted $t\bar{t}$ events	1.4 ± 0.5	1.6 ± 0.5	2.7 ± 0.8	2.0 ± 0.7	1.3 ± 0.5	1.3 ± 0.5
Fitted W+jets events	0.9 ± 0.4	0.6 ± 0.5	0.11 ± 0.08	0.08 ± 0.08	0.00 ± 0.00	$0.07^{+0.15}_{-0.07}$
Fitted diboson events	0.8 ± 0.5	0.4 ± 0.2	0.7 ± 0.4	0.10 ± 0.05	0.06 ± 0.04	0.00 ± 0.00
Fitted misidentified lepton events	$0.15^{+0.17}_{-0.15}$	0.00 ± 0.02	0.00 ± 0.01	0.00 ± 0.01	0.00 ± 0.00	0.00 ± 0.00
Fitted other background events	0.6 ± 0.3	0.09 ± 0.05	0.12 ± 0.07	0.3 ± 0.1	0.7 ± 0.3	0.3 ± 0.1
MC expected SM events	4.2 ± 1.1	2.9 ± 1.0	3.6 ± 0.9	2.4 ± 0.7	2.1 ± 0.8	1.9 ± 0.7
MC expected $t\bar{t}$ events	1.3 ± 0.4	1.5 ± 0.4	2.6 ± 0.7	1.9 ± 0.6	1.4 ± 0.5	1.4 ± 0.5
MC expected W+jets events	1.3 ± 0.5	0.9 ± 0.7	0.2 ± 0.1	0.1 ± 0.1	0.0 ± 0.0	$0.1^{+0.2}_{-0.1}$
MC expected diboson events	0.8 ± 0.5	0.4 ± 0.2	0.7 ± 0.4	0.10 ± 0.05	0.07 ± 0.04	0.00 ± 0.00
data-driven misidentified lepton events	$0.15^{+0.17}_{-0.15}$	0.00 ± 0.02	0.00 ± 0.01	0.00 ± 0.01	0.00 ± 0.00	0.00 ± 0.00
MC expected other background events	0.6 ± 0.3	0.09 ± 0.05	0.13 ± 0.07	0.3 ± 0.1	0.6 ± 0.3	0.3 ± 0.1

Table 16: Background fit results for the inclusive hard single-lepton signal regions, for an integrated luminosity of 20.3 fb^{-1}. Nominal MC expectations (normalized to MC cross-sections) are given for comparison. The uncertainties shown here combine the statistical uncertainty on the simulated event samples with the systematic uncertainties. Some categories have 0.00 ± 0.00 events, which merely reflects the fact that these categories, having no Monte Carlo events left or no input data events to the matrix method, have not been considered by the fitting procedure.

Signal channel	$\langle\epsilon\sigma\rangle^{95}_{\text{obs}}$[fb]	S^{95}_{obs}	S^{95}_{exp}	CL_B	$p(s=0)$
soft single-lepton one b-jet channels					
low-mass	0.43 (0.42)	8.8 (8.6)	$6.9^{+3.0}_{-2.0}$ ($6.9^{+3.4}_{-2.1}$)	0.76 (0.71)	0.26 (0.27)
high-mass	0.39 (0.38)	7.9 (7.7)	$6.3^{+1.9}_{-1.1}$ ($5.9^{+3.0}_{-1.9}$)	0.79 (0.75)	0.21 (0.22)
soft single-lepton two b-jet channels					
low-mass	0.66 (0.62)	13.4 (12.7)	$13.2^{+5.9}_{-4.1}$ ($13.1^{+5.6}_{-3.8}$)	0.52 (0.46)	0.50 (0.50)
high-mass	0.26 (0.24)	5.3 (4.9)	$5.3^{+2.4}_{-1.4}$ ($5.5^{+2.8}_{-1.8}$)	0.50 (0.40)	0.50 (0.50)
soft single-lepton channels					
3-jet	0.40 (0.39)	8.1 (8.1)	$7.3^{+2.7}_{-1.8}$ ($6.8^{+3.3}_{-2.1}$)	0.67 (0.66)	0.36 (0.31)
5-jet	0.35 (0.33)	7.1 (6.8)	$10.0^{+3.6}_{-3.0}$ ($9.8^{+4.2}_{-2.9}$)	0.15 (0.15)	0.50 (0.50)
soft dimuon channel	0.57 (0.54)	11.5 (11.1)	$5.9^{+2.1}_{-1.0}$ ($6.5^{+3.1}_{-1.9}$)	0.98 (0.92)	0.01 (0.02)
binned hard single-lepton channels					
3-jet (electron)	0.97 (0.98)	19.8 (19.9)	$20.2^{+8.3}_{-4.8}$ ($20.7^{+7.9}_{-5.6}$)	0.47 (0.45)	0.50 (0.50)
3-jet (muon)	0.57 (0.52)	11.6 (10.6)	$15.6^{+5.8}_{-3.8}$ ($15.8^{+6.5}_{-4.4}$)	0.13 (0.12)	0.50 (0.50)
5-jet (electron)	0.63 (0.60)	12.7 (12.1)	$12.6^{+3.2}_{-2.7}$ ($12.2^{+4.5}_{-3.2}$)	0.50 (0.49)	0.50 (0.50)
5-jet (muon)	0.38 (0.36)	7.7 (7.2)	$7.6^{+2.8}_{-2.4}$ ($7.3^{+3.4}_{-2.2}$)	0.53 (0.49)	0.50 (0.50)
6-jet (electron)	0.33 (0.34)	6.6 (6.8)	$7.8^{+3.1}_{-2.4}$ ($7.7^{+3.6}_{-2.4}$)	0.32 (0.37)	0.50 (0.50)
6-jet (muon)	0.35 (0.35)	7.1 (7.1)	$7.1^{+3.4}_{-1.4}$ ($7.4^{+3.5}_{-2.3}$)	0.50 (0.46)	0.50 (0.50)
inclusive hard single-lepton channels					
3-jet (electron)	0.30 (0.28)	6.0 (5.7)	$5.7^{+2.2}_{-1.5}$ ($5.6^{+2.9}_{-1.8}$)	0.56 (0.51)	0.48 (0.48)
3-jet (muon)	0.38 (0.37)	7.7 (7.5)	$5.1^{+2.0}_{-1.5}$ ($5.1^{+2.7}_{-1.7}$)	0.89 (0.82)	0.13 (0.13)
5-jet (electron)	0.30 (0.29)	6.0 (5.9)	$5.4^{+2.3}_{-1.5}$ ($5.5^{+2.9}_{-1.7}$)	0.60 (0.56)	0.43 (0.43)
5-jet (muon)	0.22 (0.21)	4.6 (4.2)	$4.7^{+1.9}_{-1.2}$ ($4.7^{+2.5}_{-1.6}$)	0.44 (0.41)	0.50 (0.50)
6-jet (electron)	0.23 (0.22)	4.6 (4.4)	$4.4^{+1.9}_{-0.8}$ ($4.4^{+2.5}_{-1.5}$)	0.56 (0.49)	0.50 (0.50)
6-jet (muon)	0.15 (0.12)	3.0 (2.5)	$4.1^{+1.3}_{-1.1}$ ($3.8^{+2.3}_{-1.3}$)	0.13 (0.16)	0.50 (0.50)

Table 17: Left to right: 95% CL upper limits on the visible cross section ($\langle\epsilon\sigma\rangle^{95}_{\text{obs}}$) and on the number of signal events (S^{95}_{obs}). The third column (S^{95}_{exp}) shows the 95% CL upper limit on the number of signal events, given the expected number (and $\pm1\sigma$ excursions on the expectation) of background events. The last two columns indicate the CL_B value, i.e. the confidence level observed for the background-only hypothesis, and the discovery p-value ($p(s=0)$). For an observed number of events lower than expected, the discovery p-value has been truncated at 0.5. The numbers in parentheses represent the results obtained using asymptotic analytic expressions instead of toy Monte Carlo pseudo-experiments.

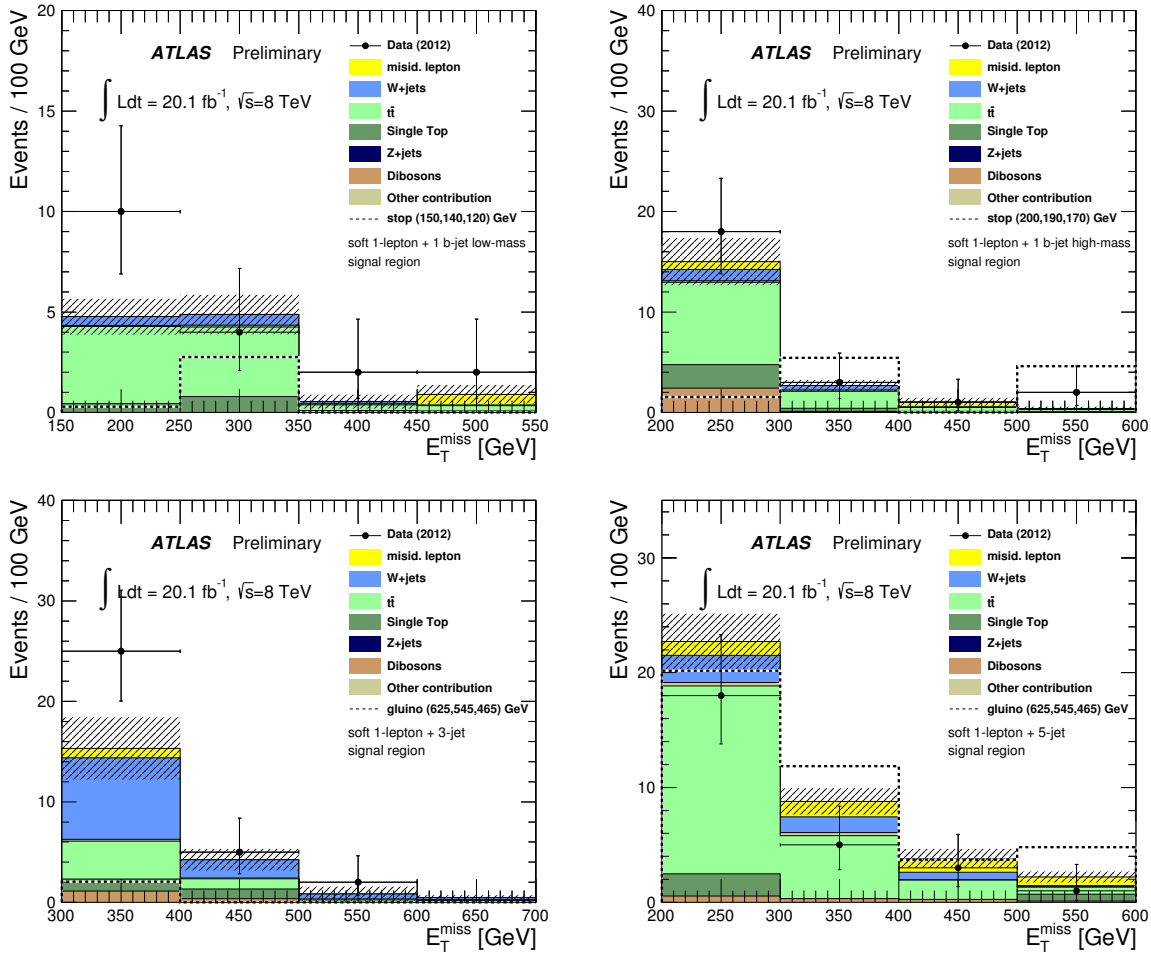

Figure 8: $E_{\mathrm{T}}^{\mathrm{miss}}$ distribution, prior to the $E_{\mathrm{T}}^{\mathrm{miss}}$ requirement, in the one b-jet low-mass (upper left) and high-mass (upper right) signal regions, the single-lepton 3-jet (bottom left) and the 5-jet (bottom right) signal regions. The Standard Model expectation is derived from the fit. The uncertainty band on the Standard Model expectation shown here combines the statistical uncertainty on the simulated event samples and the theory-related uncertainties on the background with the systematic uncertainties on the jet energy scale and resolution, on the lepton identification, momentum/energy scale and resolution, on the $E_{\mathrm{T}}^{\mathrm{miss}}$ calculation, on the b-tagging, and on the data-driven misidentified-lepton background. The last bin includes the overflow. For illustration, the expected signal distributions are shown for: top squark pair production with $m_{\tilde{t}}$=150 GeV, $m_{\tilde{\chi}_1^{\pm}}$=140 GeV and $m_{\tilde{\chi}_1^0}$=120 GeV (in the soft single-lepton one b-jet low-mass channel) and $m_{\tilde{t}}$=200 GeV, $m_{\tilde{\chi}_1^{\pm}}$=190 GeV and $m_{\tilde{\chi}_1^0}$=170 GeV (in the soft single-lepton one b-jet high-mass channel) and gluino pair production with $m_{\tilde{g}}$ = 625 GeV , $m_{\tilde{\chi}_1^{\pm}}$=545 GeV and $m_{\tilde{\chi}_1^0}$ = 465 GeV (in the single-lepton channels).

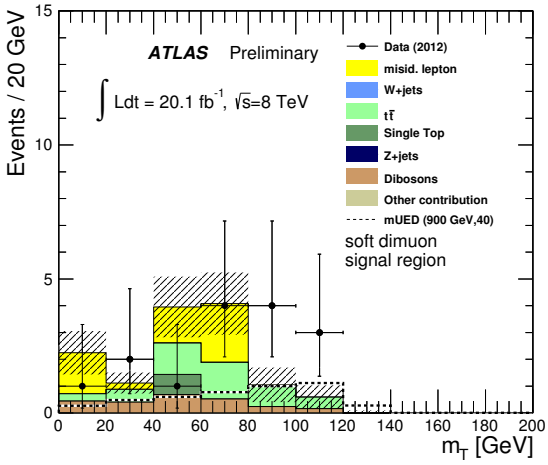

Figure 9: m_{T} distribution, prior to the m_{T} requirement, in the soft dimuon signal region. The Standard Model expectation is derived from the fit. The uncertainty band on the Standard Model expectation shown here combines the statistical uncertainty on the simulated event samples and the theory-related uncertainties on the background with the systematic uncertainties on the jet energy scale and resolution, on the lepton identification, momentum/energy scale and resolution, on the $E_{\mathrm{T}}^{\mathrm{miss}}$ calculation, on the b-tagging, and on the data-driven misidentified-lepton background. The last bin includes the overflow. For illustration, the expected signal distribution is shown for the mUED model point with R = 900 GeV and ΛR=40.

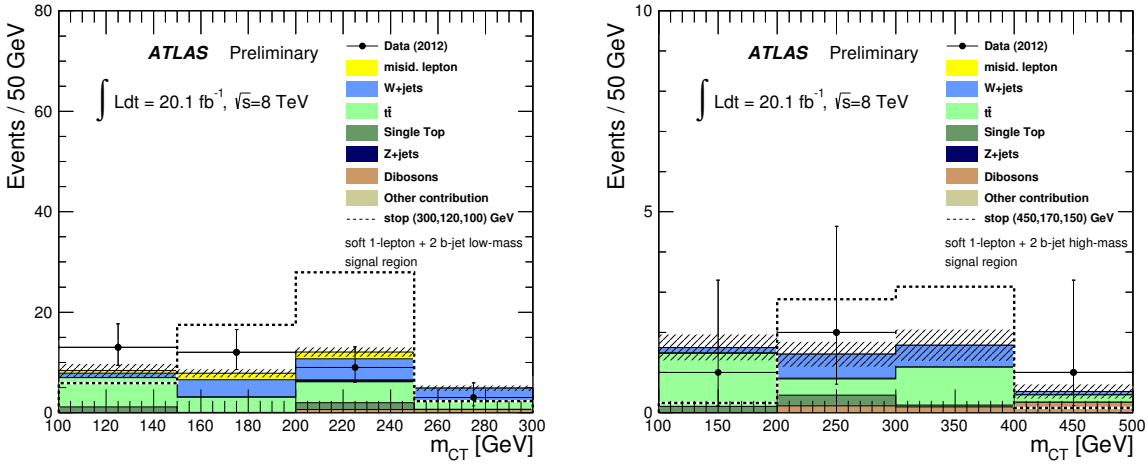

Figure 10: m_{CT} distribution, prior to the m_{CT} requirement, in the two b-jet low-mass (left) and high-mass (right) signal regions. The Standard Model expectation is derived from the fit. The uncertainty band on the Standard Model expectation shown here combines the statistical uncertainty on the simulated event samples and the theory-related uncertainties on the background with the systematic uncertainties on the jet energy scale and resolution, on the lepton identification, momentum/energy scale and resolution, on the $E_{\mathrm{T}}^{\mathrm{miss}}$ calculation, on the b-tagging, and on the data-driven misidentified-lepton background. The last bin includes the overflow. For illustration, the expected signal distributions are shown for top squark pair production with $m_{\tilde{t}}$=300 GeV, $m_{\tilde{\chi}_1^{\pm}}$=120 GeV and $m_{\tilde{\chi}_1^0}$=100 GeV (in the low-mass channel) and $m_{\tilde{t}}$=450 GeV, $m_{\tilde{\chi}_1^{\pm}}$=170 GeV and $m_{\tilde{\chi}_1^0}$=150 GeV (in the high-mass channel).

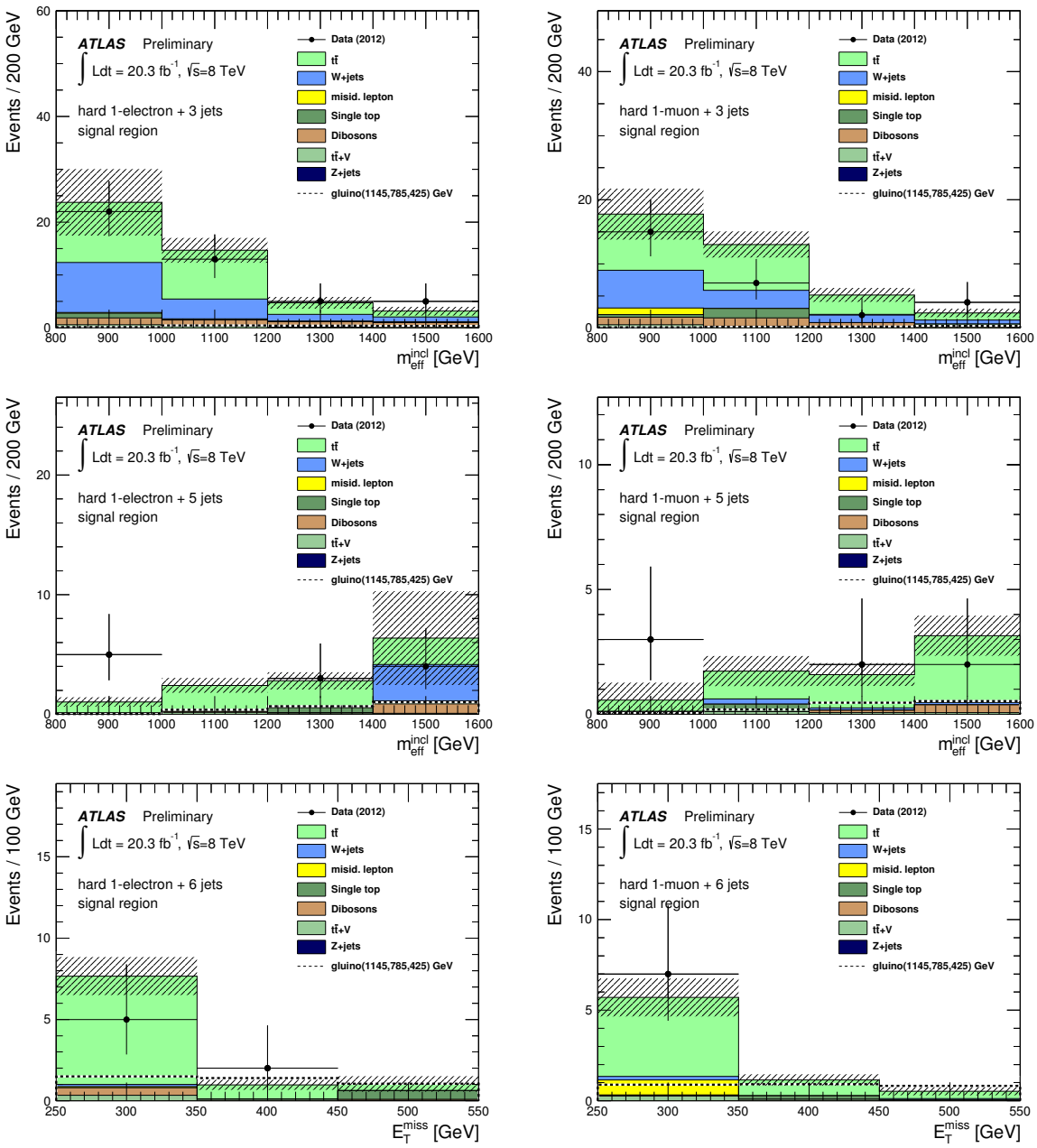

Figure 11: $m_{\mathrm{eff}}^{\mathrm{incl}}$ distribution in the electron (left) and muon (right) channels in the hard single-lepton 3-jet (top) and 5-jet (middle) binned signal regions. The bottom plots show the $E_{\mathrm{T}}^{\mathrm{miss}}$ distribution in the electron (left) and muon (right) channels in the hard single-lepton 6-jet binned signal region. The Standard Model expectation is derived from the fit. The uncertainty band on the Standard Model expectation shown here combines the statistical uncertainty on the simulated event samples and the theory-related uncertainties on the background with the systematic uncertainties on the jet energy scale and resolution, on the lepton identification, momentum/energy scale and resolution, on the $E_{\mathrm{T}}^{\mathrm{miss}}$ calculation, on the b-tagging, and on the data-driven misidentified-lepton background. The last bin includes the overflow. For illustration, the expected signal distributions are shown for one-step gluino pair production with $m_{\tilde{g}}$=1145 GeV, $m_{\tilde{\chi}_1^{\pm}}$=785 GeV and $m_{\tilde{\chi}_1^0}$=425 GeV.

Given the absence of a significant excess above the Standard Model background expectations, limits can also be placed on the various specific models of physics beyond the Standard Model described in Section 3. In this case, the fit is modified in the following way:

1. there is an extra free parameter for a possible non-SM signal strength which is constrained to be non-negative;

2. the number of events observed in the signal region is now also considered as an input to the fit;

3. the expected contamination of the control regions by the signal is included in the fit.

For the hard-lepton channel, the binned signal regions are used; the likelihood is modified to take into account the model $m_{\rm eff}^{\rm inc}$ ($E_{\rm T}^{\rm miss}$) shape information in the signal regions as a further discriminant by dividing the 3-jet and 5-jet (6-jet) signal regions into four (three) equidistant bins, from 800 GeV to 1600 GeV (from 250 GeV to 550 GeV), with the last bin being inclusive for higher values, and by including bin-by-bin expectations. In these exclusion fits, the statistically independent electron and muon channels are combined.

Systematic uncertainties on the signal expectations stemming from detector effects are included in the fit in the same way as for the backgrounds. Systematic uncertainties on the signal cross section due to the choice of renormalization and factorization scale and PDF uncertainties are calculated following the procedure described in [46] and their effect is shown on the limit plots obtained.

The limits in the $m_0 - m_{1/2}$ MSUGRA/CMSSM plane obtained from the hard-lepton signal regions are shown in Figure 12. The observed limit is driven above the expected limit (although within the 1σ band) mainly by the shape fit to the $E_{\rm T}^{\rm miss}$ distribution in the 6-jet binned signal region (see Figure 11) as some high-$E_{\rm T}^{\rm miss}$ bins are found to be without data events. At large values of m_0, this analysis is able to exclude a gluino mass of up to 1.2 TeV. This is approximately 100 GeV more than the analysis based on large jet multiplicites and $E_{\rm T}^{\rm miss}$ with no lepton in the final state [90].

The limits obtained from the combination of all soft and hard single-lepton signal regions are shown in Figures 13 for the gluino and the squark pair production simplified models. These limits are shown in the $m_{\tilde{g}(\tilde{q})}$–$m_{\tilde{\chi}_1^0}$ mass plane for the case in which the chargino mass is fixed at $x = 1/2$, where $x = (m_{\tilde{\chi}_1^\pm} - m_{\tilde{\chi}_1^0})/(m_{\tilde{g}(\tilde{q})} - m_{\tilde{\chi}_1^0})$. These limits are obtained by using, for each point of the mass plane, the soft or the hard single-lepton limit, selecting the best expected limit for this point. The soft single-lepton analysis is particularly powerful along the diagonal, where the masses of the gluino/squark and the lightest neutralino are almost degenerate. In this region, the limit on the gluino mass reaches up to $m_{\tilde{g}} = 700$ GeV for all values of the lightest neutralino mass for which the gluino/neutralino mass difference is greater than 25 GeV. This extends the previous limit [16] by approximately 150 GeV in $m_{\tilde{g}}$ for a $\Delta m(\tilde{g}, \tilde{\chi}_1^0)$ of approximately 100 GeV. The hard-lepton analysis is able to exclude a gluino mass up to 1.18 TeV in this model, extending the previous limit by 200 GeV for low $\tilde{\chi}_1^0$ masses while covering a considerably larger range of $\Delta m(\tilde{g}, \tilde{\chi}_1^0)$. The squark limits are considerably weaker due to the lower production cross section. This analysis nevertheless extends the limit on the squark mass from this model to approximately 700 GeV, or 200 GeV above the previous limit. The upper limit on the production cross section for each point considered is also shown.

The limits are also shown in Figure 14 for the gluino/squark simplified models in which the LSP mass is set at 60 GeV and the value of x is varied. In these models, the hard single-lepton searches exclude up to $m_{\tilde{g}} = 1.2$ TeV and this exclusion covers a wide range of chargino masses; these searches also exclude squark masses up to 750 GeV, albeit for a slightly narrower range of chargino masses. With respect to the previously published limits, the exclusion is increase by 250 GeV in the gluino mass and 200 GeV in the squark mass.

In the two-step gluino/squark simplified models with sleptons, the limits obtained using the hard single-lepton analyses are shown in Figure 15. Gluino and squark masses up to 1.15 TeV and 750

GeV are excluded, respectively. These searches are also able to exclude a gluino mass up to 1.12 TeV in the two-step simplified model without sleptons, as can be seen in Figure 16, although the exclusion curve does not reach the same level of spectrum compression in this model as in the model with sleptons. Figure 16 also shows the upper limit on the production cross section on each point considered in the two-step squark simplified model without sleptons.

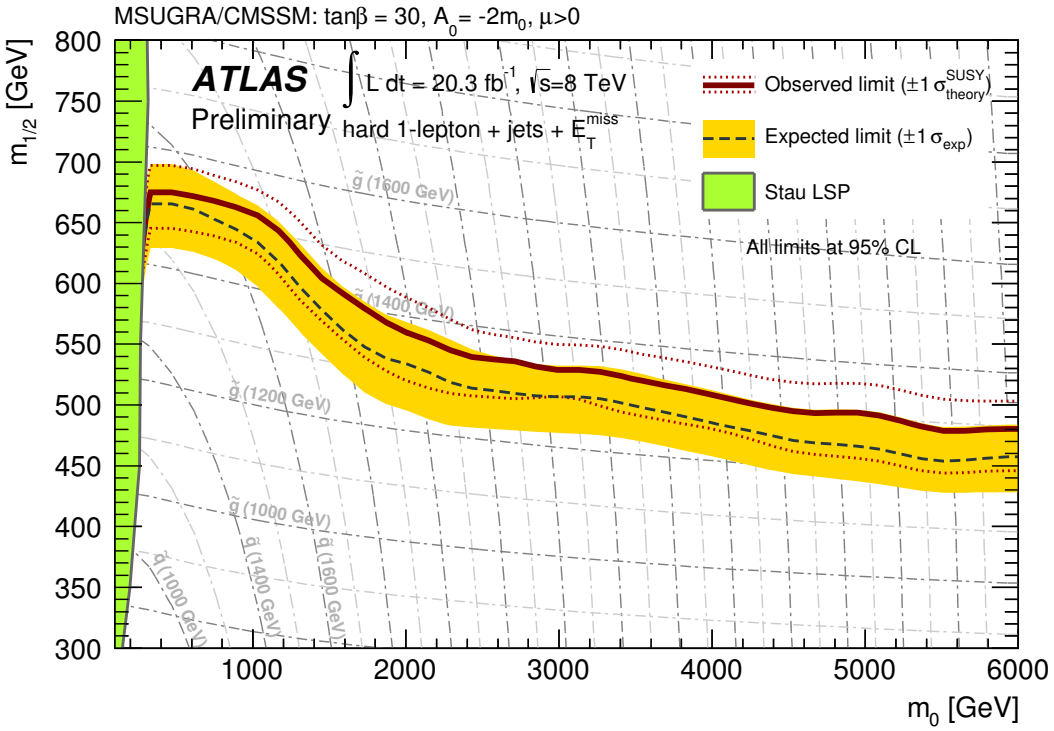

Figure 12: 95% CL exclusion limit from the hard single-lepton channels in the $m_0 - m_{1/2}$ MSUGRA/CMSSM plane with $\tan\beta = 30$, $A_0 = -2m_0$ and $\mu > 0$. The green area represents the region of the parameter space for which the stau is the LSP. The dark grey dashed line shows the expected limits at 95% CL, with the light (yellow) bands indicating the $\pm 1\sigma$ variation on the median expected limit due to the experimental and background-theory uncertainties. The observed nominal limit is indicated by a solid dark red line with the dark red dotted lines being obtained by varying the signal cross section by the scale and PDF uncertainties.

The limits obtained for the top squark production simplified models with almost degenerate $\tilde{\chi}_1^{\pm}$ and $\tilde{\chi}_1^0$ are shown in Figure 17 in the $m_{\tilde{t}}$–$m_{\tilde{\chi}_1^0}$ mass plane, for the following two assumptions: $\Delta m(\tilde{\chi}_1^{\pm}, \tilde{\chi}_1^0) = 5$ (top) or 20 GeV(bottom). These limits are obtained by using, for each point of the mass plane, the low-mass or the high-mass soft single-lepton two b-jet signal region, selecting the best expected limit for this point. The limits extend up to $m_{\tilde{t}} = 420$ (450) GeV in the $\Delta m(\tilde{\chi}_1^{\pm}, \tilde{\chi}_1^0) = 5$ (20) GeV scenario. The soft single-lepton one b-jet signal regions do not result in an exclusion limit in these models. The upper limit on the production cross section placed on each point considered in the $m_{\tilde{t}}$–$m_{\tilde{\chi}_1^0}$ mass plane can be found in the Appendix (Figure 22).

The limit obtained for the mUED scenario using the soft dimuon signal region is shown in Figure 18 in the $1/R$–ΛR plane. Given the small excess in this channel, the limit obtained only reaches up to a compactification radius of $1/R = 740$ GeV for a cut-off scale times radius (ΛR) of approximately 10.

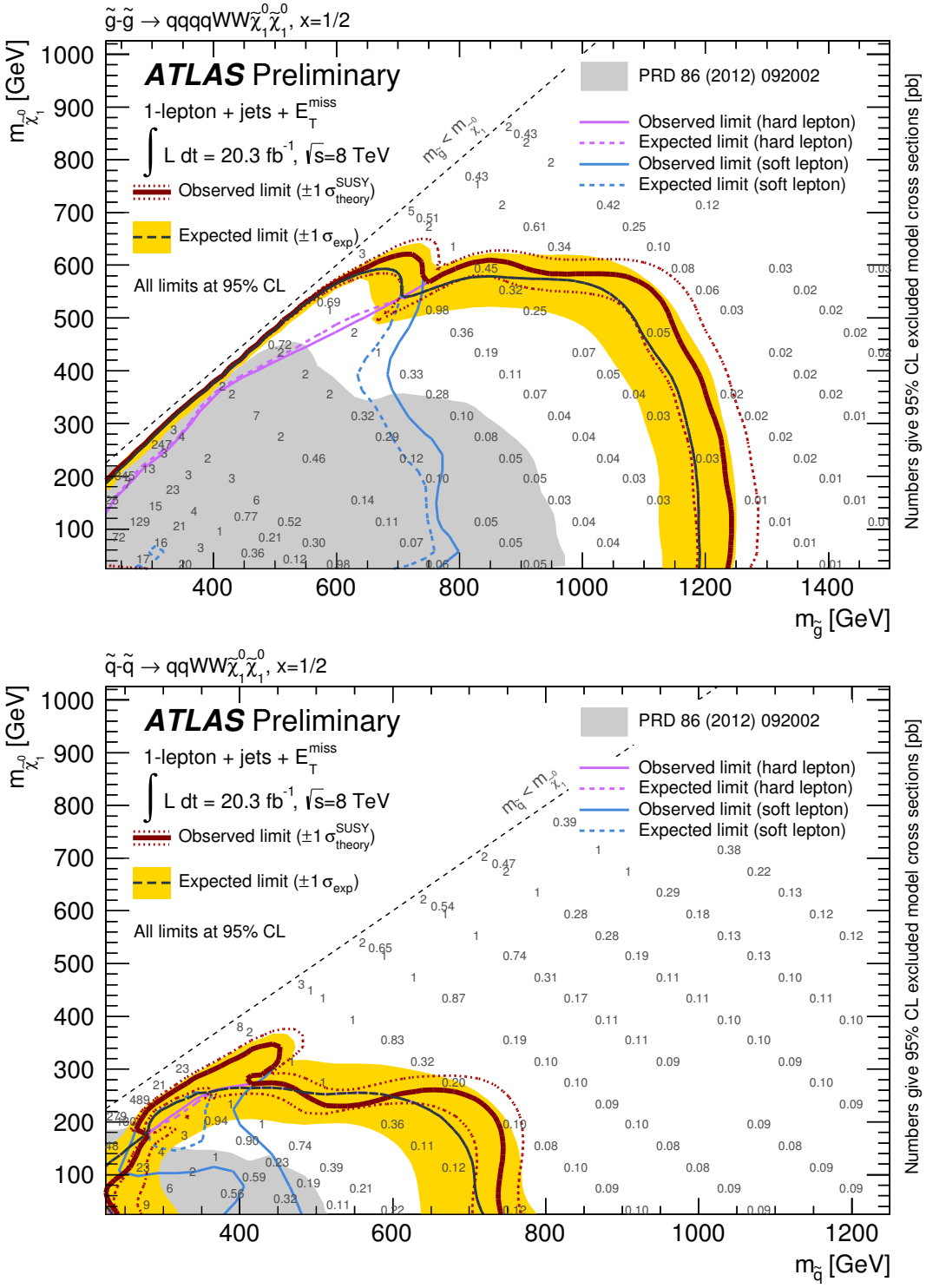

Figure 13: 95% CL exclusion limit from the single-lepton channels in the gluino simplified model (top) and the first and second generation squark simplified model (bottom) presented in the $m_{\tilde{g}(\tilde{q})}$–$m_{\tilde{\chi}_1^0}$ mass plane for the case in which the chargino mass is fixed at $x = 1/2$, where $x = (m_{\tilde{\chi}_1^\pm} - m_{\tilde{\chi}_1^0})/(m_{\tilde{g}(\tilde{q})} - m_{\tilde{\chi}_1^0})$. The dark grey dashed line shows the expected limits at 95% CL, with the light (yellow) bands indicating the $\pm 1\sigma$ variation on the median expected limit due to the experimental and background-theory uncertainties. The observed nominal limit is indicated by a solid dark red line with the dark red dotted lines being obtained by varying the signal cross section by the scale and PDF uncertainties. The observed limit set by the previous ATLAS analysis [16] using 7 TeV data is shown as a grey area. The light blue and purple full (dashed) lines show the observed (expected) exclusion obtained by the soft and hard-lepton analyses, respectively. The grey numbers show the upper limit on the production cross section, in pb, obtained for each point of the grids.

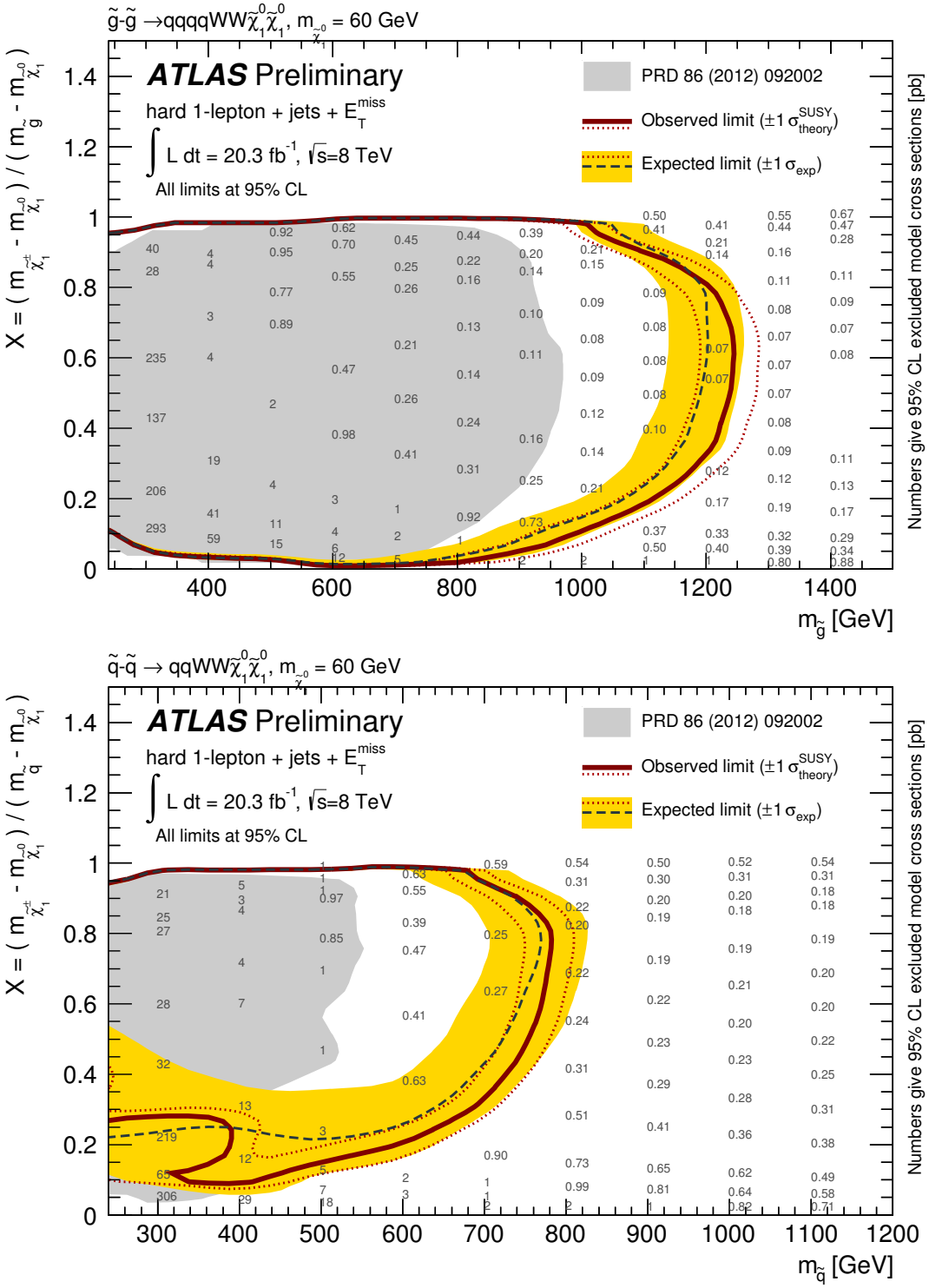

Figure 14: 95% CL exclusion limit from the hard single-lepton channels in the gluino simplified model (top) and the first and second generation squark simplified model (bottom) presented in the $m_{\tilde{g}(\tilde{q})}$–x mass plane, where $x = (m_{\tilde{\chi}_1^\pm} - m_{\tilde{\chi}_1^0})/(m_{\tilde{g}(\tilde{q})} - m_{\tilde{\chi}_1^0})$, for the case in which the chargino mass is varied and the LSP mass is set at 60 GeV. The dark grey dashed line shows the expected limits at 95% CL, with the light (yellow) bands indicating the $\pm1\sigma$ variation on the median expected limit due to the experimental and background-theory uncertainties. The observed nominal limit is indicated by a solid dark red line with the dark red dotted lines being obtained by varying the signal cross section by the scale and PDF uncertainties. The observed limit set by the previous ATLAS analysis [16] using 7 TeV data is shown as a grey area. The grey numbers show the upper limit on the production cross section, in pb, obtained for each point of the grids.

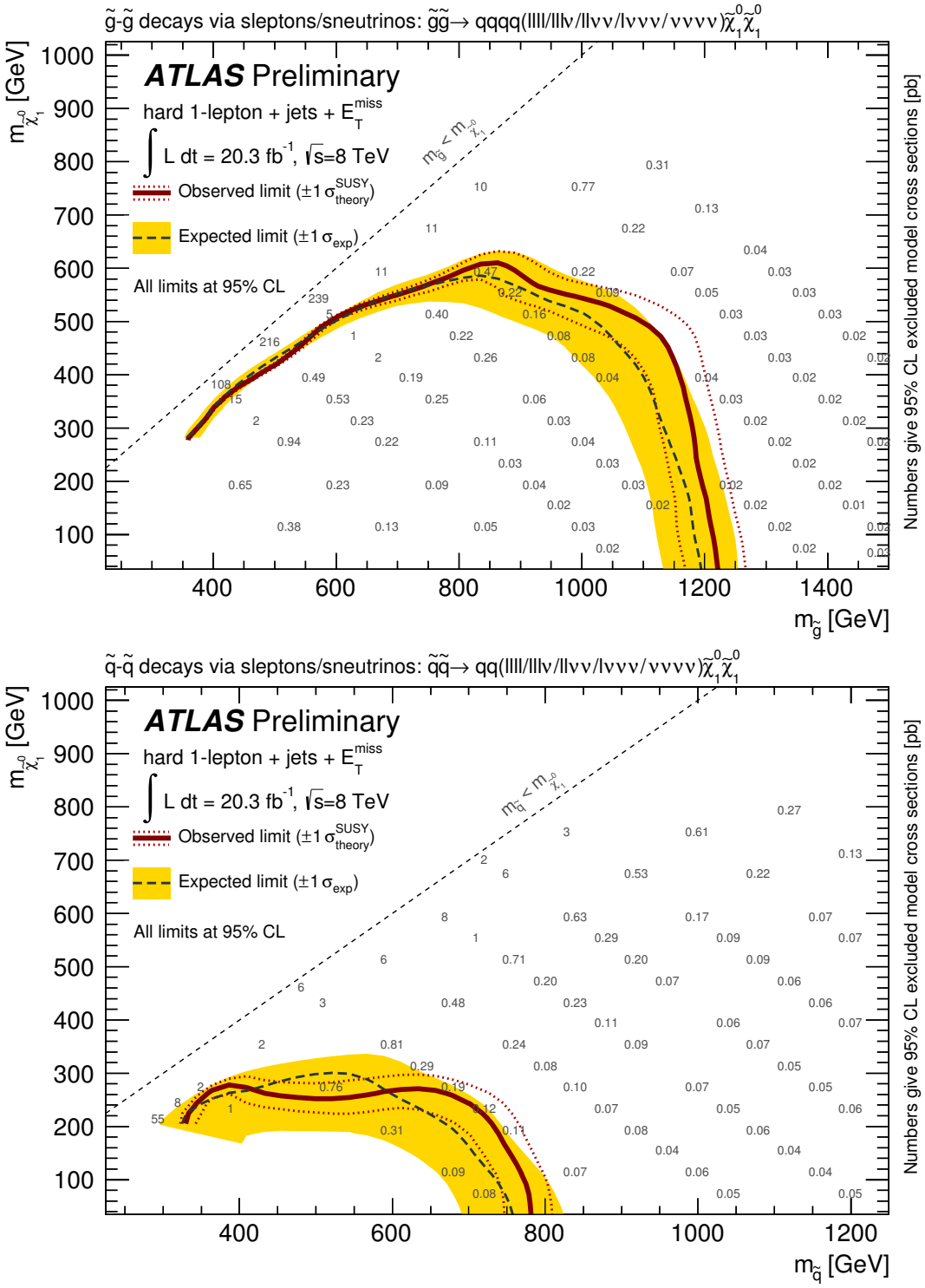

Figure 15: 95% CL exclusion limit from the hard single-lepton channels in the two-step gluino simplified model with sleptons (top) and the two-step first and second generation squark simplified model with sleptons (bottom) presented in the $m_{\tilde{g}(\tilde{q})}$–$m_{\tilde{\chi}_1^0}$ mass plane. The dark grey dashed line shows the expected limits at 95% CL, with the light (yellow) bands indicating the $\pm 1\sigma$ variation on the median expected limit due to the experimental and background-theory uncertainties. The observed nominal limit is indicated by a solid dark red line with the dark red dotted lines being obtained by varying the signal cross section by the scale and PDF uncertainties. The grey numbers show the upper limit on the production cross section, in pb, obtained for each point of the grids. The limit is not extrapolated to lower gluino/squark masses where no grid point was generated.

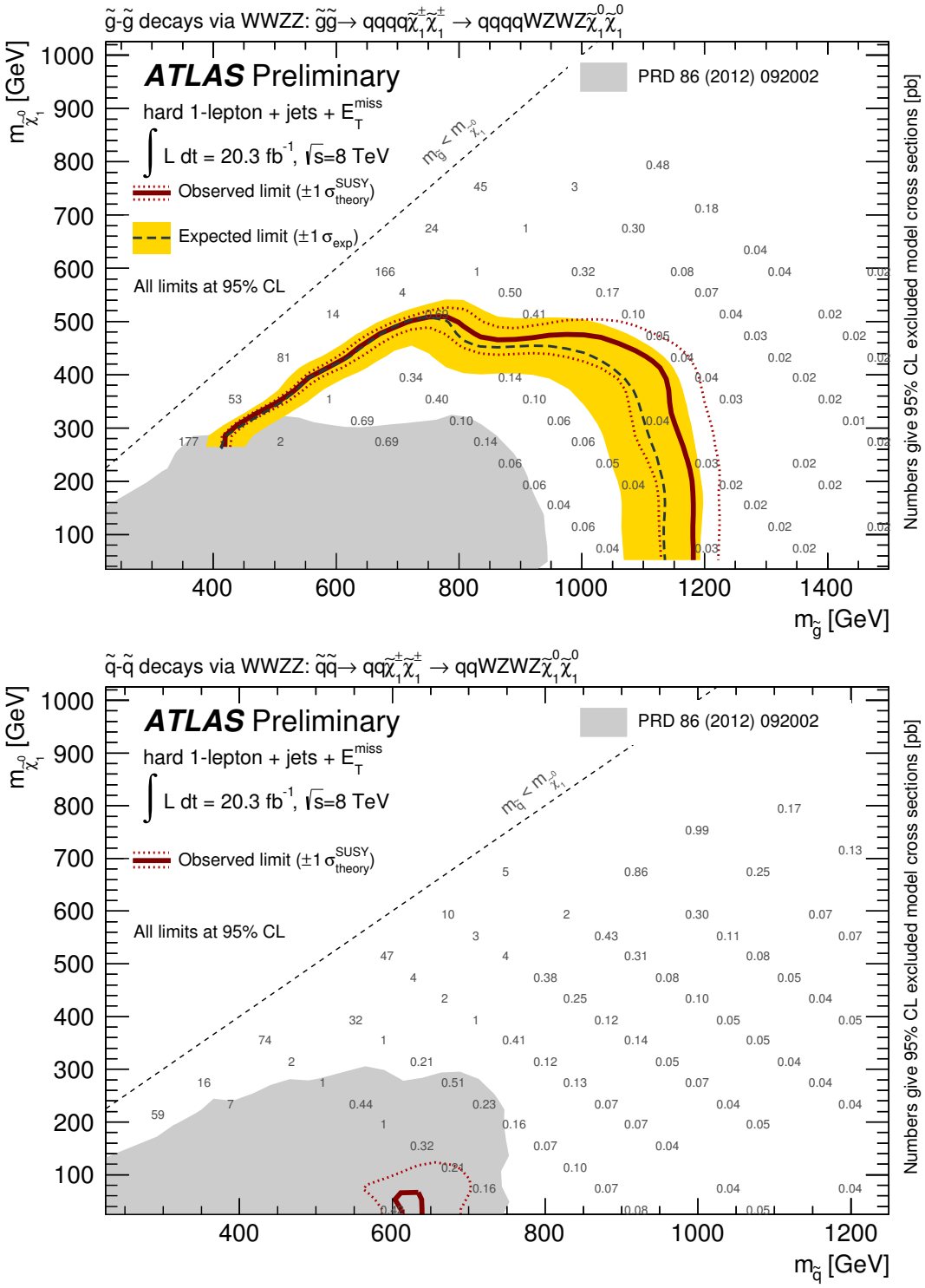

Figure 16: 95% CL exclusion limit from the hard single-lepton channels in the two-step gluino simplified model without sleptons presented in the $m_{\tilde{g}}$–$m_{\tilde{\chi}_1^0}$ mass plane (top) and in the two-step first and second generation squark simplified model without sleptons (bottom). The dark grey dashed line shows the expected limits at 95% CL, with the light (yellow) bands indicating the $\pm 1\sigma$ variation on the median expected limit due to the experimental and background-theory uncertainties. The observed nominal limit is indicated by a solid dark red line with the dark red dotted lines being obtained by varying the signal cross section by the scale and PDF uncertainties. The grey numbers show the upper limit on the production cross section, in pb, obtained for each point of the grids. The limit is not extrapolated to lower gluino/neutralino masses where no grid point was generated.

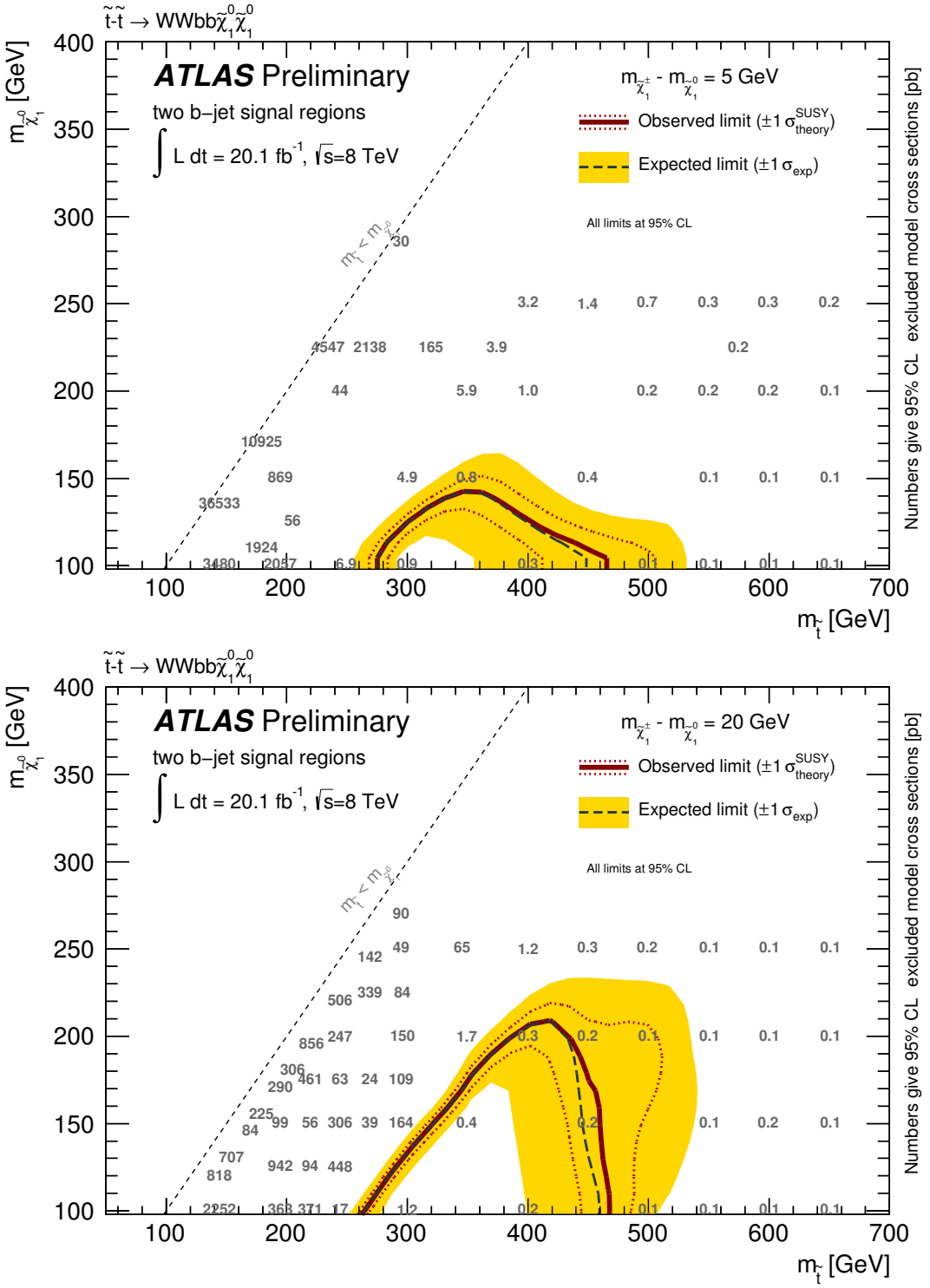

Figure 17: 95% CL exclusion limit from the soft single-lepton two b-jet channels in the top squark pair production simplified model, presented in the $m_{\tilde{t}}$–$m_{\tilde{\chi}_1^0}$ mass plane for the case in which the mass difference between the lighter chargino and the LSP is 5 GeV (top) or 20 GeV (bottom). The dark grey dashed line shows the expected limits at 95% CL, with the light (yellow) bands indicating the $\pm 1\sigma$ variation on the median expected limit due to the experimental and background-theory uncertainties. The observed nominal limit is indicated by a solid dark red line with the dark red dotted lines being obtained by varying the signal cross section by the scale and PDF uncertainties. The grey numbers show the upper limit on the production cross section, in pb, obtained for each point of the grids.

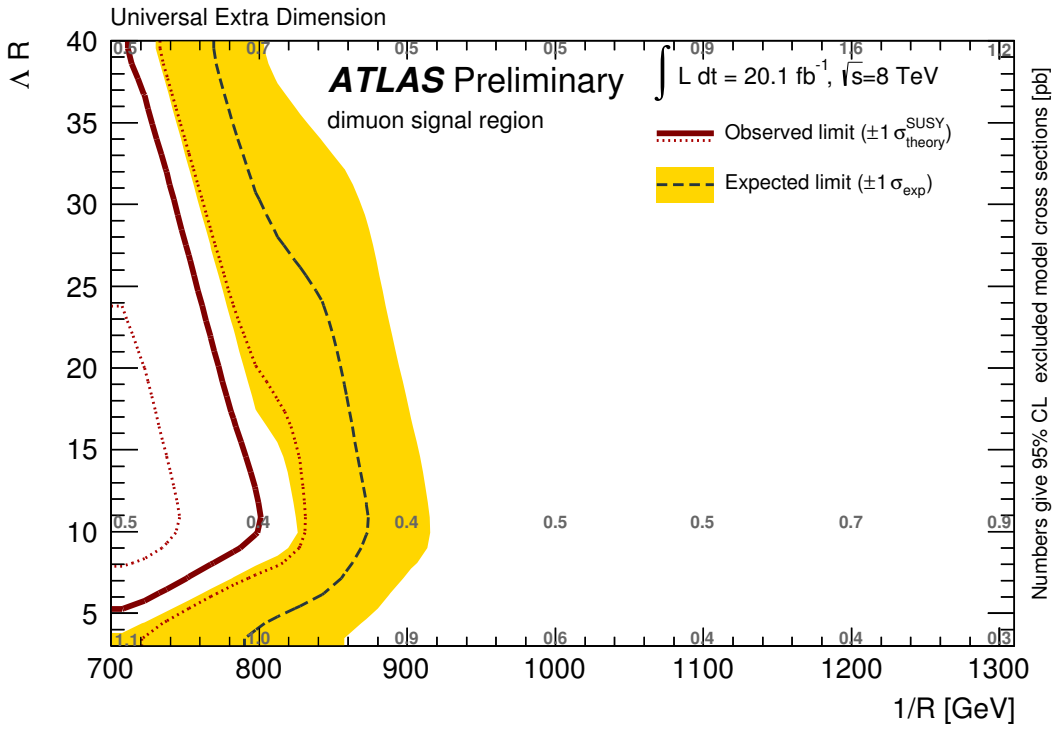

Figure 18: 95% CL exclusion limit from the soft dimuon channel in the mUED model, presented in the $1/R$–ΛR plane. The dark grey dashed line shows the expected limits at 95% CL, with the light (yellow) bands indicating the $\pm 1\sigma$ variation on the median expected limit due to the experimental and background-theory uncertainties. The observed nominal limit is indicated by a solid dark red line with the dark red dotted lines being obtained by varying the signal cross section by the scale and PDF uncertainties. The grey numbers show the upper limit on the production cross section, in pb, obtained for each point of the grids.

11 Conclusion

A search with the ATLAS detector for SUSY in final states containing at least one isolated lepton (electron or muon), jets and large missing transverse momentum is presented in this note, using 19 different signal regions. The kinematic reach of the analysis is extended to soft leptons to increase the sensitivity to supersymmetric spectra with small mass splitting. This analysis uses 20 fb^{-1} of data collected at a center-of-mass energy of 8 TeV. Observations are in general in good agreement with the Standard Model background expectations, although a non-significant excess (at 2.3σ) is seen in the soft dimuon channel. Limits are set on the visible cross section of new physics within the kinematic requirements of the searches. Limits are also set on a variety of models. A gluino mass up to 1.1-1.2 TeV can be excluded in a MSUGRA/CMSSM scenario at high values of m_0 and in the one-step and two-step gluino simplified models considered. First and second generation squark masses up to 700-750 GeV are also excluded in the one-step and two-step squark simplified models studied. Limits are also set on a top squark pair production simplified model with nearly degenerate $\tilde{\chi}_1^0$ and $\tilde{\chi}_1^\pm$, as expected in a natural scenario where $\tilde{\chi}_1^\pm$ and $\tilde{\chi}_1^0$ are higgsino-like. In the simplified scenario considered, the top squark decays exclusively into the lighter chargino and a b-quark. Depending on the chargino and neutralino masses, the analysis excludes a top squark mass up to 450 GeV. Finally, limits are also set in the mUED model, excluding a compactification radius up to $1/R = 740$ GeV, depending on ΛR.

References

[1] H. Miyazawa, *Baryon Number Changing Currents*, Prog. Theor. Phys. **36 (6)** (1966) 1266–1276.

[2] P. Ramond, *Dual Theory for Free Fermions*, Phys. Rev. **D3** (1971) 2415–2418.

[3] Y. A. Golfand and E. P. Likhtman, *Extension of the Algebra of Poincare Group Generators and Violation of p Invariance*, JETP Lett. **13** (1971) 323–326. [Pisma Zh. Eksp. Teor. Fiz. 13:452-455,1971].

[4] A. Neveu and J. H. Schwarz, *Factorizable dual model of pions*, Nucl. Phys. **B31** (1971) 86–112.

[5] A. Neveu and J. H. Schwarz, *Quark Model of Dual Pions*, Phys. Rev. **D4** (1971) 1109–1111.

[6] J. Gervais and B. Sakita, *Field theory interpretation of supergauges in dual models*, Nucl. Phys. **B34** (1971) 632–639.

[7] D. V. Volkov and V. P. Akulov, *Is the Neutrino a Goldstone Particle?*, Phys. Lett. **B46** (1973) 109–110.

[8] J. Wess and B. Zumino, *A Lagrangian Model Invariant Under Supergauge Transformations*, Phys. Lett. **B49** (1974) 52.

[9] J. Wess and B. Zumino, *Supergauge Transformations in Four-Dimensions*, Nucl. Phys. **B70** (1974) 39–50.

[10] L. Evans and P. Bryant (editors), *LHC Machine*, JINST **3** (2008) S08001.

[11] P. Fayet, *Supersymmetry and Weak, Electromagnetic and Strong Interactions*, Phys. Lett. **B64** (1976) 159.

[12] P. Fayet, *Spontaneously Broken Supersymmetric Theories of Weak, Electromagnetic and Strong Interactions*, Phys. Lett. **B69** (1977) 489.

[13] G. R. Farrar and P. Fayet, *Phenomenology of the Production, Decay, and Detection of New Hadronic States Associated with Supersymmetry*, Phys. Lett. **B76** (1978) 575–579.

[14] P. Fayet, *Relations Between the Masses of the Superpartners of Leptons and Quarks, the Goldstino Couplings and the Neutral Currents*, Phys. Lett. **B84** (1979) 416.

[15] S. Dimopoulos and H. Georgi, *Softly Broken Supersymmetry and SU(5)*, Nucl. Phys. **B193** (1981) 150.

[16] ATLAS Collaboration, *Further search for supersymmetry at $\sqrt{s}$ = 7 TeV in final states with jets, missing transverse momentum and isolated leptons with the ATLAS detector*, Phys. Rev **D86** (2012) 092002, arXiv:1208.4688 [hep-ex].

[17] CMS Collaboration, *Search for supersymmetry in events with a single lepton and jets using templates*, CMS-PAS-SUS-11-027 (2012) . (http://cdsweb.cern.ch/record/1449810).

[18] ATLAS Collaboration, *Search for supersymmetry at $\sqrt{s}$=8 TeV in final states with jets, missing transverse momentum and one isolated lepton*, ATLAS-CONF-2012-104 (2012) . (http://cds.cern.ch/record/1472673).

[19] ATLAS Collaboration, *The ATLAS Experiment at the CERN Large Hadron Collider*, JINST **3** (2008) S08003.

[20] ATLAS Collaboration, *Expected Performance of the ATLAS Experiment - Detector, Trigger and Physics*, arXiv:0901.0512 [hep-ex].

[21] J. Alwall, P. Schuster, and N. Toro, *Simplified Models for a First Characterization of New Physics at the LHC*, Phys. Rev. **D79** (2009) 075020, arXiv:0810.3921 [hep-ph].

[22] D. Alves et al., *Simplified Models for LHC New Physics Searches*, J. Phys. G: Nucl. Part. Phys. **39** (2012) 105005, arXiv:1105.2838 [hep-ph].

[23] A.H. Chamseddine, R.L. Arnowitt and P. Nath, Phys. Rev. Lett. **49** (1982) 970; R. Barbieri, S. Ferrara and C.A. Savoy, Phys. Lett. **B119** (1982) 343; L.E. Ibanez, Phys. Lett. **B118** (1982) 73; L.J. Hall, J.D. Lykken and S. Weinberg, Phys. Rev. **D27** (1983) 2359; N. Ohta, Prog. Theor. Phys. **70** (1983) 542.

[24] G. L. Kane, C. F. Kolda, L. Roszkowski, and J. D. Wells, *Study of constrained minimal supersymmetry*, Phys. Rev. **D49** (1994) 6173–6210, arXiv:hep-ph/9312272 [hep-ph].

[25] H.-C. Cheng, K. Matchev, and M. Schmaltz, *Bosonic Supersymmetry? Getting Fooled at the LHC*, Phys. Rev. **D66** (2002) 56006.

[26] ATLAS Collaboration, *Search for squarks and gluinos with the ATLAS detector in final states with jets and missing transverse momentum and 20.3 fb^{-1} of $\sqrt{s}$ = 8 TeV proton-proton collision data*, ATLAS-CONF-2013-047 (2013) . http://cds.cern.ch/record/1547563.

[27] R. Barbieri and G. Giudice, *Upper Bounds on Supersymmetric Particle Masses*, Nucl.Phys. **B306** (1988) 63.

[28] B. de Carlos and J. Casas, *One loop analysis of the electroweak breaking in supersymmetric models and the fine tuning problem*, Phys.Lett. **B309** (1993) 320–328, arXiv:hep-ph/9303291 [hep-ph].

[29] LEP SUSY Working Group (ALEPH, DELPHI, L3,OPAL), Notes LEPSUSYWG/01-03.1 and 04-01.1, http://lepsusy.web.cern.ch/lepsusy/Welcome.html.

[30] ATLAS Collaboration, *Search for direct third generation squark pair production in final states with missing transverse momentum and two b-jets in* $\sqrt{s} = 8$ *TeV pp collisions with the ATLAS detector.*, ATLAS-CONF-2013-053 (2013) . http://cds.cern.ch/record/1547570.

[31] J. Alwall, M. Herquet, F. Maltoni, O. Mattelaer, and T. Stelzer, *MadGraph 5 : Going Beyond*, JHEP **1106** (2011) 128, arXiv:1106.0522 [hep-ph].

[32] T. Sjostrand, S. Mrenna, and P. Skands, *PYTHIA 6.4 physics and manual*, JHEP **05** (2006) 026, arXiv:hep-ph/0603175.

[33] J. Pumplin et al., *New generation of parton distributions with uncertainties from global QCD analysis*, JHEP **0207** (2002) 012, arXiv:hep-ph/0201195 [hep-ph].

[34] J. Alwall et al., *Comparative study of various algorithms for the merging of parton showers and matrix elements in hadronic collisions*, Eur. Phys. J. **C53** (2008) 473–500, arXiv:0706.2569 [hep-ph].

[35] ATLAS Collaboration, *New ATLAS event generator tunes to 2010 data*, ATL-PHYS-PUB-2011-008 (2011) . (http://cdsweb.cern.ch/record/1345343).

[36] M. Bahr et al., *Herwig++ Physics and Manual*, Eur. Phys. J. **C58** (2008) 639–707, arXiv:0803.0883 [hep-ph].

[37] A. Djouadi, M. Muhlleitner, and M. Spira, *Decays of supersymmetric particles: The Program SUSY-HIT (SUspect-SdecaY-Hdecay-InTerface)*, Acta Phys. Polon. **B38** (2007) 635–644, arXiv:hep-ph/0609292.

[38] B. C. Allanach, *SOFTSUSY: a program for calculating supersymmetric spectra*, Comput. Phys. Commun. **143** (2002) 305–331, arXiv:hep-ph/0104145.

[39] M. Muhlleitner, A. Djouadi, and Y. Mambrini, *SDECAY: A Fortran code for the decays of the supersymmetric particles in the MSSM*, Comput. Phys. Commun. **168** (2005) 46–70, arXiv:hep-ph/0311167.

[40] S. Gieseke, C. Rohr, and A. Siodmok, *Colour reconnections in Herwig++*, Eur.Phys.J. **C72** (2012) 2225, arXiv:1206.0041 [hep-ph].

[41] W. Beenakker, R. Hopker, M. Spira, and P. Zerwas, *Squark and gluino production at hadron colliders*, Nucl. Phys. **B492** (1997) 51–103, arXiv:hep-ph/9610490 [hep-ph].

[42] A. Kulesza and L. Motyka, *Threshold resummation for squark-antisquark and gluino-pair production at the LHC*, Phys. Rev. Lett. **102** (2009) 111802, arXiv:0807.2405 [hep-ph].

[43] A. Kulesza and L. Motyka, *Soft gluon resummation for the production of gluino-gluino and squark-antisquark pairs at the LHC*, Phys. Rev. **D80** (2009) 095004, arXiv:0905.4749 [hep-ph].

[44] W. Beenakker et al., *Soft-gluon resummation for squark and gluino hadroproduction*, JHEP **0912** (2009) 041, arXiv:0909.4418 [hep-ph].

[45] W. Beenakker et al., *Squark and gluino hadroproduction*, Int. J. Mod. Phys. **A26** (2011) 2637–2664, arXiv:1105.1110 [hep-ph].

[46] M. Kramer et al., *Supersymmetry production cross sections in pp collisions at $\sqrt{s}$ = 7 TeV*, arXiv:1206.2892 [hep-ph].

[47] T. Gleisberg et al., *Event generation with Sherpa 1.1*, JHEP **02** (2009) 007, 0811.4622 [hep-ph].

[48] K. Melnikov and F. Petriello, *Electroweak gauge boson production at hadron colliders through O(alpha(s)**2)*, Phys. Rev. **D74** (2006) 114017, arXiv:hep-ph/0609070 [hep-ph].

[49] M. L. Mangano, M. Moretti, F. Piccinini, R. Pittau, and A. D. Polosa, *ALPGEN, a generator for hard multiparton processes in hadronic collisions*, JHEP **0307** (2003) 001, arXiv:hep-ph/0206293 [hep-ph].

[50] S. Frixione, P. Nason, and G. Ridolfi JHEP **0709** (2007) 126, arXiv:hep-ph/0707.3088.

[51] M. Aliev et al., *HATHOR: HAdronic Top and Heavy quarks crOss section calculatoR*, Comput. Phys. Commun. **182** (2011) 1034–1046, arXiv:1007.1327 [hep-ph].

[52] B. P. Kersevan and E. Richter-Was, *The Monte Carlo event generator AcerMC version 2.0 with interfaces to PYTHIA 6.2 and HERWIG 6.5*, arXiv:hep-ph/0405247 [hep-ph].

[53] N. Kidonakis, *Next-to-next-to-leading-order collinear and soft gluon corrections for t-channel single top quark production*, Phys. Rev. **D83** (2011) 091503, arXiv:1103.2792 [hep-ph].

[54] S. Frixione and B. R. Webber, *Matching NLO QCD computations and parton shower simulations*, JHEP **0206** (2002) 029, arXiv:hep-ph/0204244 [hep-ph].

[55] N. Kidonakis, *NNLL resummation for s-channel single top quark production*, Phys. Rev. **D81** (2010) 054028, arXiv:1001.5034 [hep-ph].

[56] N. Kidonakis, *Two-loop soft anomalous dimensions for single top quark associated production with a W- or H-*, Phys. Rev. **D82** (2010) 054018, arXiv:1005.4451 [hep-ph].

[57] J. M. Campbell, R. Ellis, and D. L. Rainwater, *Next-to-leading order QCD predictions for W + 2 jet and Z + 2 jet production at the CERN LHC*, Phys. Rev. **D68** (2003) 094021, arXiv:hep-ph/0308195 [hep-ph].

[58] J. M. Campbell and R. K. Ellis JHEP **1207** (2012) 052, arXiv:hep-ph/1204.5678 [hep-ph].

[59] A. Lazopoulos, T. McElmurry, K. Melnikov, and F. Petriello Phys.Lett. **B666** (2008) 62, arXiv:hep-ph/0804.2220 [hep-ph].

[60] G. Corcella et al., *HERWIG 6: An Event generator for hadron emission reactions with interfering gluons (including supersymmetric processes)*, JHEP **0101** (2001) 010, arXiv:hep-ph/0011363 [hep-ph].

[61] J. Butterworth, J. R. Forshaw, and M. Seymour, *Multiparton interactions in photoproduction at HERA*, Z. Phys. **C72** (1996) 637–646, arXiv:hep-ph/9601371 [hep-ph].

[62] H.-L. Lai et al., *New parton distributions for collider physics*, Phys. Rev. **D82** (2010) 074024, arXiv:1007.2241 [hep-ph].

[63] S. Catani, L. Cieri, G. Ferrera, D. de Florian, M. Grazzini, Phys. Rev. Lett. 103 082001 (2009), arXiv:0903.2120 [hep-ph]; S. Catani, M. Grazzini, Phys. Rev. Lett. 98 222002 (2007) hep-ph/0703012.

[64] A. Martin, W. Stirling, R. Thorne, and G. Watt, *Update of parton distributions at NNLO*, Phys. Lett. **B652** (2007) 292–299, arXiv:0706.0459 [hep-ph].

[65] ATLAS Collaboration, *The ATLAS Simulation Infrastructure*, Eur. Phys. J. **C70** (2010) 823–874, arXiv:1005.4568 [physics.ins-det].

[66] GEANT4 Collaboration, S. Agostinelli et al., *GEANT4: A Simulation toolkit*, Nucl. Instrum. Meth. **A506** (2003) 250–303.

[67] ATLAS Collaboration, *The simulation principle and performance of the ATLAS fast calorimeter simulation FastCaloSim*, ATL-PHYS-PUB-2010-013 (2010) . (http://cds.cern.ch/record/1300517).

[68] ATLAS Collaboration, *Improved luminosity determination in pp collisions at $\sqrt{s}$ = 7 TeV using the ATLAS detector at the LHC*, arXiv:1302.4393 [hep-ex]. (Submitted to EPJC).

[69] ATLAS Collaboration, *Performance of primary vertex reconstruction in proton-proton collisions at $\sqrt{s}$ = 7 TeV in the ATLAS experiment*, ATLAS-CONF-2010-069 (2010) . (http://cdsweb.cern.ch/record/1281344).

[70] M. Cacciari, G. P. Salam, and G. Soyez, *The anti-k_t jet clustering algorithm*, JHEP **04** (2008) 063, arXiv:0802.1189 [hep-ph].

[71] M. Cacciari and G. P. Salam, *Dispelling the N^3 myth for the k_t jet-finder*, Phys. Lett. **B641** (2006) 57–61, arXiv:hep-ph/0512210.

[72] ATLAS Collaboration, *Jet energy measurement with the ATLAS detector in proton-proton collisions at $\sqrt{s}$ = 7 TeV*, Eur. Phys. J. **C73 3** (2013) 2304, arXiv:1112.6426 [hep-ex].

[73] ATLAS Collaboration, *Single hadron response measurement and calorimeter jet energy scale uncertainty with the ATLAS detector at the LHC*, arXiv:1203.1302 [hep-ex].

[74] ATLAS Collaboration, *Electron performance measurements with the ATLAS detector using the 2010 LHC proton-proton collision data*, arXiv:1110.3174 [hep-ex].

[75] ATLAS Collaboration. https://atlas.web.cern.ch/Atlas/GROUPS/PHYSICS/EGAMMA/PublicPlots/20121403/EfficiencyPileupATL-COM-PHYS-2012-260/index.html.

[76] ATLAS Collaboration, *A measurement of the ATLAS muon reconstruction and trigger efficiency using J/psi decays*, ATLAS-CONF-2011-021 (2011) . (http://cdsweb.cern.ch/record/1336750).

[77] ATLAS Collaboration, *Muon reconstruction efficiency in reprocessed 2010 LHC proton-proton collision data recorded with the ATLAS detector*, ATLAS-CONF-2011-063 (2011) . (http://cdsweb.cern.ch/record/1345743).

[78] ATLAS Collaboration, *Search for supersymmetry in final states with jets, missing transverse momentum and one isolated lepton in $\sqrt{s}$ = 7 TeV collisions using 1 fb^{-1} of ATLAS data*, Phys. Rev. **D85** (2012) 012006.

[79] ATLAS Collaboration, *Performance of Missing Transverse Momentum Reconstruction in Proton-Proton Collisions at 7 TeV with ATLAS*, Eur. Phys. J. **C72** (2012) 1844, arXiv:1108.5602 [hep-ex].

[80] ATLAS Collaboration, *Commissioning of the ATLAS high-performance b-tagging algorithms in the 7 TeV collision data*, ATLAS-CONF-2011-102 (2011) . (http://cdsweb.cern.ch/record/1369219).

[81] ATLAS Collaboration, *Measurement of the b-tag Efficiency in a Sample of Jets Containing Muons with 5 fb^{-1} of Data from the ATLAS Detector*, ATLAS-CONF-2012-043 (2012) . (http://cdsweb.cern.ch/record/1435197).

[82] D. R. Tovey, *On measuring the masses of pair-produced semi-invisibly decaying particles at hadron colliders*, JHEP **0804** (2008) 034, arXiv:0802.2879 [hep-ph].

[83] G. Polesello and D. R. Tovey, *Supersymmetric particle mass measurement with the boost-corrected contransverse mass*, JHEP **1003** (2010) 030, arXiv:0910.0174 [hep-ph].

[84] ATLAS Collaboration, *Search for direct production of charginos and neutralinos in events with three leptons and missing transverse momentum in 21 fb^{-1} of pp collisions at $\sqrt{s}$ = 8 TeV with the ATLAS detector*, ATLAS-CONF-2013-035 (2013) . http://cds.cern.ch/record/1532426.

[85] ATLAS Collaboration, *Jet energy resolution and selection efficiency relative to track jets from in-situ techniques with the ATLAS Detector Using Proton-Proton Collisions at a Center of Mass Energy $\sqrt{s}$ = 7 TeV*, ATLAS-CONF-2010-054 (2010) . (http://cdsweb.cern.ch/record/1281311).

[86] ATLAS Collaboration, *Measurement of the Mistag Rate of b-tagging algorithms with 5 fb^{-1} of Data Collected by the ATLAS Detector*, ATLAS-CONF-2012-040 (2012) . (http://cdsweb.cern.ch/record/1435194).

[87] ATLAS Collaboration, *Measurement of the cross-section for W boson production in association with b-jets in pp collisions at $\sqrt{s}$ = 7 TeV with the ATLAS detector*, arXiv:1302.2929 [hep-ex] (2013) . Submitted to JHEP.

[88] G. Cowan, K. Cranmer, E. Gross, and O. Vitells, *Asymptotic formulae for likelihood-based tests of new physics*, Eur. Phys. J. **C71** (2011) 1554, arXiv:1007.1727 [physics.data-an].

[89] A. L. Read, *Presentation of search results: The CL(s) technique*, J. Phys. G **G28** (2002) 2693–2704.

[90] ATLAS Collaboration, *Search for new phenomena using final states with large jet multiplicities and missing transverse momentum with ATLAS in 20 fb^{-1} of $\sqrt{s}$ = 8 TeV proton-proton collisions*, ATLAS-CONF-2013-054 (2013) . http://cds.cern.ch/record/1547571.

A Appendix

A.1 Additional plots

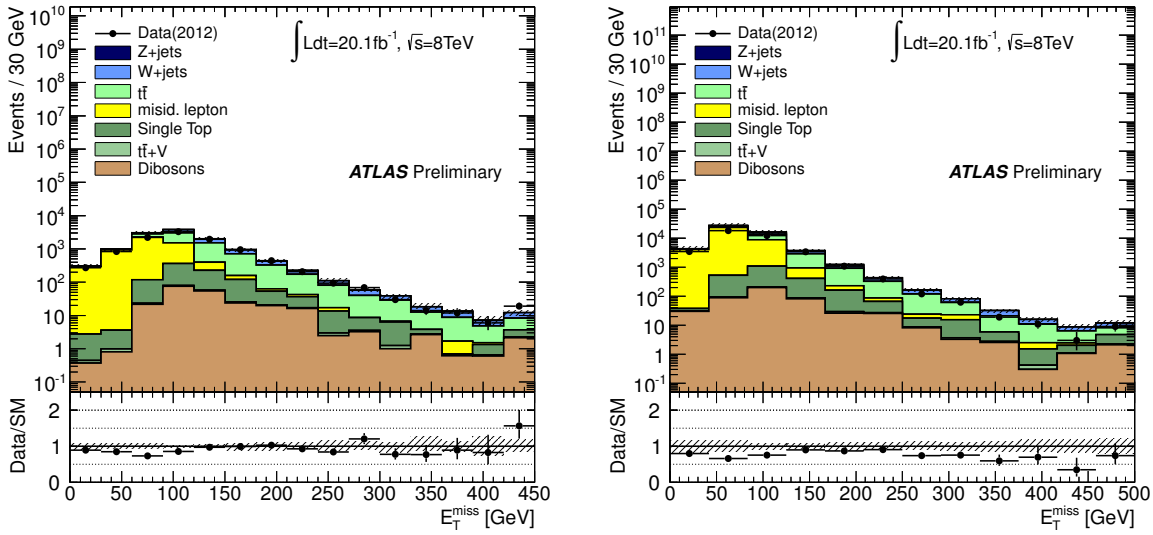

Figure 19: $E_{\mathrm{T}}^{\mathrm{miss}}$ distribution in the electron (left) and muon (right) channels for events passing the $E_{\mathrm{T}}^{\mathrm{miss}}$ trigger and having exaclty one preselected soft lepton, at least one b-jet with $p_{\mathrm{T}}>$ 25 GeV and $m_{\mathrm{T}}<$ 30 GeV. This region is used to validate the data-driven misidentified lepton background estimation. The "Data/SM" plots show the ratio between data and the summed Standard Model expectation. The remaining Standard Model expectation is derived from simulation only, normalized to the theoretical cross sections. The uncertainty band on the Standard Model expectation shown here combines the statistical uncertainty on the simulated event samples with the systematic uncertainties on the jet energy scale and resolution, on the lepton identification, momentum/energy scale and resolution, on the $E_{\mathrm{T}}^{\mathrm{miss}}$ calculation, on the b-tagging, and on the data-driven misidentified-lepton background.

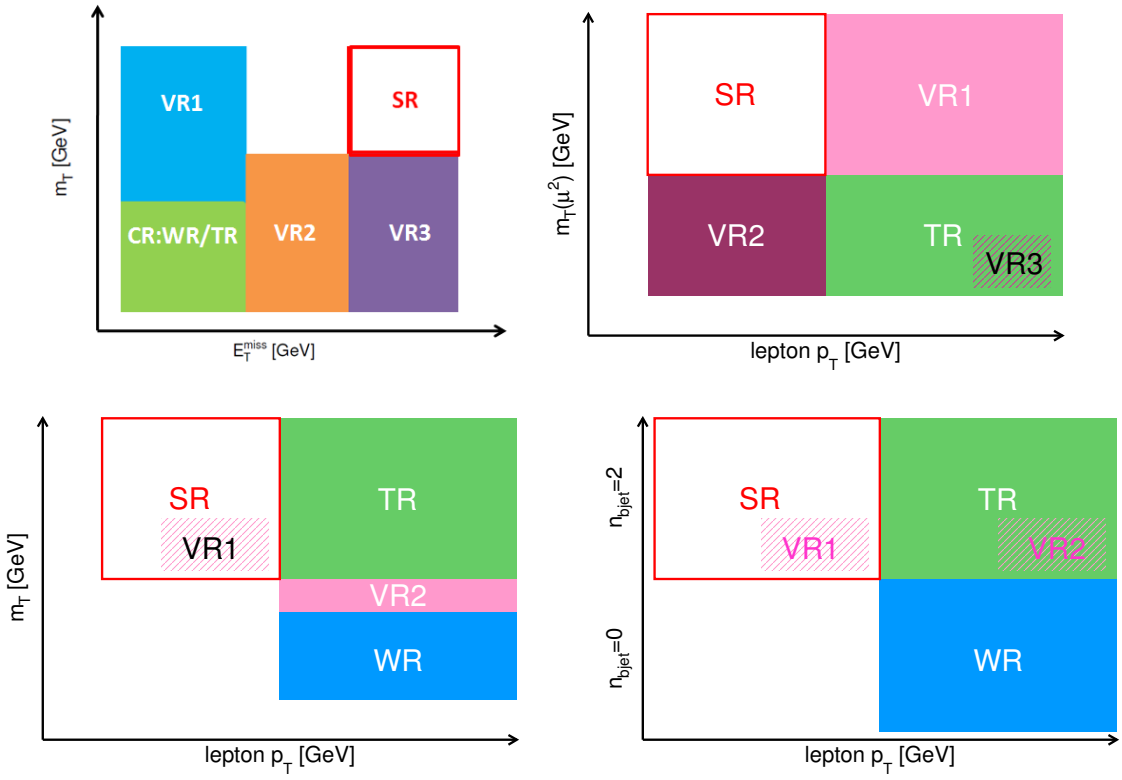

Figure 20: Graphical illustration of the soft-lepton signal regions used in this analysis. The soft single-lepton signal region is shown in the m_{T} versus $E_{\mathrm{T}}^{\mathrm{miss}}$ plane (top left), the soft dimuon signal region, in the m_{T} versus the lepton p_{T} plane (top right), the soft single-lepton one b-jet signal region, in the m_{T} versus the lepton p_{T} plane (bottom left) and the soft single-lepton two b-jet signal region, in the $n_{b-\mathrm{jet}}$ versus the lepton p_{T} plane (bottom right). The control and validation regions used are also shown.

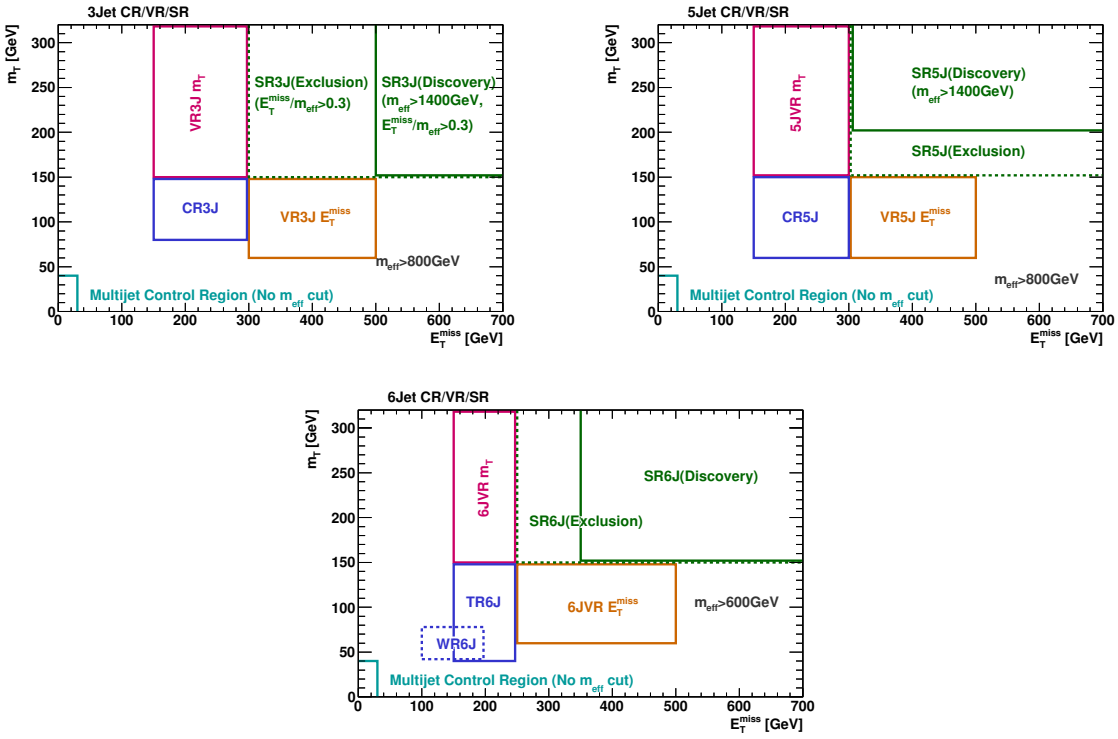

Figure 21: Graphical illustration of the hard-lepton 3-jet (top left), 5-jet (top right) and 6-jet (bottom) signal regions used in this analysis, shown in the m_{T} versus $E_{\mathrm{T}}^{\mathrm{miss}}$ plane. The control and validation regions used are also shown.

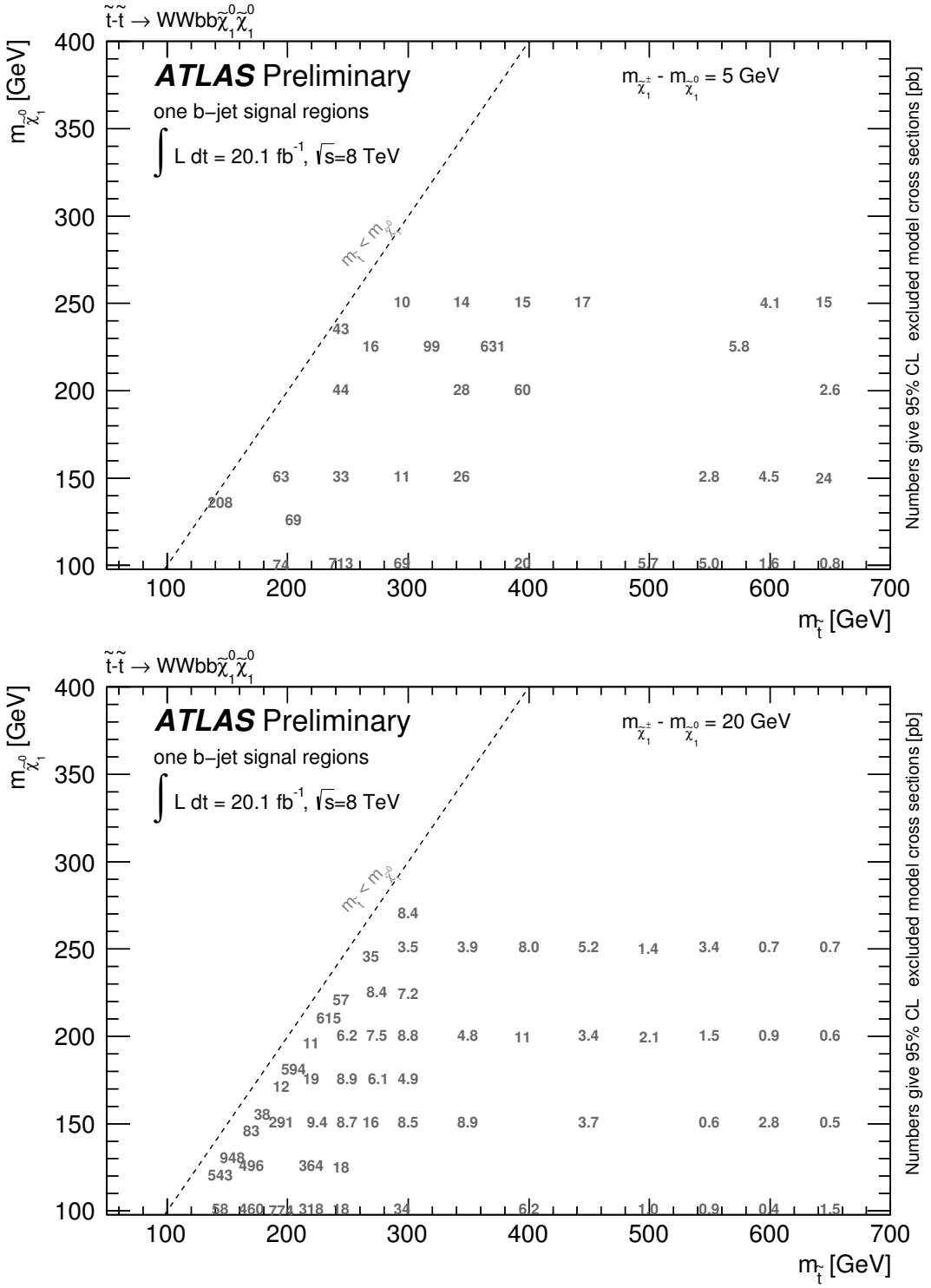

Figure 22: Upper limit on the cross section, in pb, obtained from the soft single-lepton one b-jet signal regions in the top squark pair production simplified model, presented in the $m_{\tilde{t}}$–$m_{\tilde{\chi}_1^0}$ mass plane for the case in which the mass difference between the lighter chargino and the LSP is 5 GeV (top) or 20 GeV (bottom).

A.2 Models studied

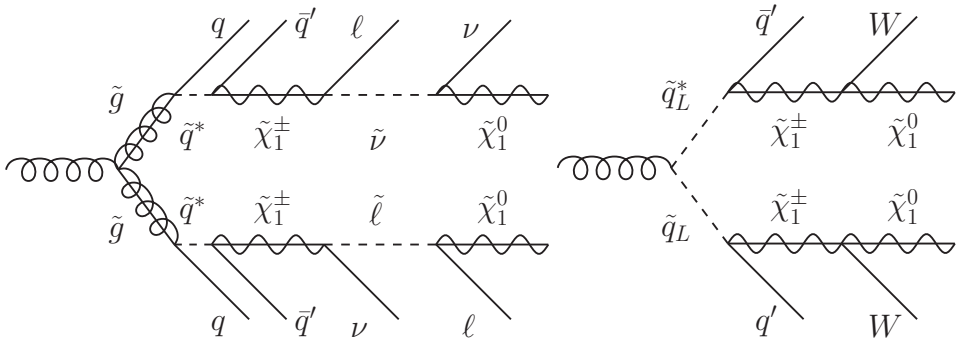

Figure 23: The decay topologies of some models considered in this analysis: the two-step gluino simplified model with sleptons (left) and the one-step squark simplified model (right).

A.3 Cut flow tables for benchmark signal models

Additional details are provided here for the benchmark signal models used in this note: cut flow charts for each signal regions are given in Tables 18-23.

Cut	Signal ($m_{\tilde{t}}$=150 GeV, $m_{\tilde{\chi}_1^\pm}$=140 GeV, $m_{\tilde{\chi}_1^0}$=120 GeV)
Trigger+soft lepton (incl. $\Delta R_{\min}(j,\ell) > 1.0$)	23391
$E_{\mathrm{T}}^{\mathrm{miss}} > 250$ GeV	515
$p_{T,\mathrm{jet1}} > 180$ GeV	498
$m_{\mathrm{T}} > 100$ GeV	22.6
$N_{\mathrm{jets}} \geq 3$	14.1
$b$tag requirement	3.0
$E_{\mathrm{T}}^{\mathrm{miss}}/m_{\mathrm{eff}} > 0.35$	3.0

Table 18: Cut flow chart for the low-mass soft single-lepton one b-jet channel; 100000 events were generated for this signal point with a truth-level $E_{\mathrm{T}}^{\mathrm{miss}}$ filter at 60 GeV. The events are normalized to 20.1 fb^{-1}.

Cut	Signal ($m_{\tilde{t}}$=200 GeV, $m_{\tilde{\chi}_1^\pm}$=190 GeV, $m_{\tilde{\chi}_1^0}$=170 GeV)
Trigger+soft lepton (incl. $\Delta R_{\min}(j,\ell) > 1.0$)	7485
$E_{\mathrm{T}}^{\mathrm{miss}} > 300$ GeV	266.5
$p_{T,\mathrm{jet1}} > 180$ GeV	248.2
$m_{\mathrm{T}} > 100$ GeV	34.2
$N_{\mathrm{jets}} \geq 3$	19.9
$b$tag requirement	11.0
$E_{\mathrm{T}}^{\mathrm{miss}}/m_{\mathrm{eff}} > 0.35$	10.0

Table 19: Cut flow chart for the high-mass soft single-lepton one b-jet channel; 100000 events were generated for this signal point with a truth-level $E_{\mathrm{T}}^{\mathrm{miss}}$ filter at 60 GeV. The events are normalized to 20.1 fb^{-1}.

Cut	Signal ($m_{\tilde{t}}$=300 GeV, $m_{\tilde{\chi}_1^\pm}$= 120 GeV, $m_{\tilde{\chi}_1^0}$=100 GeV)
Trigger+soft lepton	3692
$E_{\mathrm{T}}^{\mathrm{miss}} > 200$ GeV	772
$N_{bjet} == 2$	67.0
$\Delta\phi_{\min} > 0.4$	66.3
$m_{\mathrm{CT}} > 150$ GeV	55.8
$H_{T,2} < 50$ GeV	47.6

Table 20: Cut flow chart for the low-mass soft single-lepton two b-jet channel; 100000 events were generated for this signal point with a truth-level $E_{\mathrm{T}}^{\mathrm{miss}}$ filter at 60 GeV. The events are normalized to 20.1 fb^{-1}.

Cut	Signal ($m_{\tilde{t}}$=450 GeV, $m_{\tilde{\chi}_1^\pm}$=170 GeV, $m_{\tilde{\chi}_1^0}$=150 GeV)
Trigger+soft lepton	400
$E_{\mathrm{T}}^{\mathrm{miss}} > 300$ GeV	77.3
$N_{bjets} == 2$	6.4
$\Delta\phi_{\min} > 0.4$	6.3
$m_{\mathrm{CT}} > 200$ GeV	6.1

Table 21: Cut flow chart for the high-mass soft single-lepton two b-jet channel; 30000 events were generated for this signal point with a truth-level $E_{\mathrm{T}}^{\mathrm{miss}}$ filter at 60 GeV. The events are normalized to 20.1 fb^{-1}.

Cut	Signal ($m_{\tilde{g}}$=625 GeV, $m_{\tilde{\chi}_1^0}$=465 GeV)	Signal ($m_{\tilde{q}}$=425 GeV, $m_{\tilde{\chi}_1^0}$=345 GeV)
Common preselection		
Trigger+soft lepton	688	947
$E_{\mathrm{T}}^{\mathrm{miss}} > 200$ GeV and $p_{\mathrm{T}}{}^{j_1} > 180$ GeV	150	202
3-jet signal region		
$3 \leq N_{jet} < 5$	37.4	95.6
m_{T}> 100 GeV	7.2	15.7
All cuts	0	3.0
5-jet signal region		
$N_{jet} \geq 5$	111	78
m_{T}> 100 GeV	51.2	27.2
All cuts	19.5	12.1

Table 22: Cut flow chart for the single-lepton 3-jet and 5-jet channels. The signal points are taken from the simplified model with $x = 1/2$; 20000 (60000) events were generated for the gluino (squark) signal point. The events are normalized to 20.1 fb^{-1}.

Cut	Signal (R^{-1} = 900 GeV, ΛR=40)
trigger + OS μ	161
$E_{\mathrm{T}}^{\mathrm{miss}}$ >170 GeV	63.3
$N_{\mathrm{jets}}(p_T > 25) \geq 2$	62.2
$p_{T,\mathrm{jet1}} > 70$ GeV	61.9
$m_{\mu\mu}$ >15 GeV, $\lvert m_{\mu\mu} - m_Z \rvert$ >10 GeV	58.1
$\Delta R_{min}(j, \ell_2) > 1.0$	36.0
$p_T^{\mu 1}$ <25 GeV	5.2
m_{T}> 80 GeV	2.8
b-veto	2.4

Table 23: Cut flow chart for the soft dimuon channel; 20000 events were generated for this signal points, using a filter requiring at least 2 leptons at truth level with p_{T}> 5 GeV and $|\eta| < 2.8$. The events are normalized to 20.1 fb^{-1}.

Cut	Signal ($m_{\tilde{g}}$ = 1145 GeV, $m_{\tilde{\chi}_1^\pm}$ = 785 GeV, $m_{\tilde{\chi}_1^0}$ = 425 GeV)
Trigger + hard-lepton	18.7
Jets cut	8.1
Jet orthogonality	8.1
$E_{\mathrm{T}}^{\mathrm{miss}}$	5.2
m_{T}	4.1
$E_{\mathrm{T}}^{\mathrm{miss}}/m_{\mathrm{eff}}^{\mathrm{excl}}$	4.1
$m_{\mathrm{eff}}^{\mathrm{incl}}$	4.1

Table 24: Cut flow chart for the hard single-lepton 6-jet electron channel. The signal point is taken from the gluino simplified model with $x = 1/2$; 20000 events were generated for this point. The events are normalized to 20.3 fb^{-1}.

Cut	Signal ($m_{\tilde{g}}$ = 1145 GeV, $m_{\tilde{\chi}_1^\pm}$ = 785 GeV, $m_{\tilde{\chi}_1^0}$ = 425 GeV)
Trigger + hard-lepton	13.0
Jets cut	5.7
Jet orthogonality	5.7
$E_{\mathrm{T}}^{\mathrm{miss}}$	3.8
m_{T}	2.8
$E_{\mathrm{T}}^{\mathrm{miss}}/m_{\mathrm{eff}}^{\mathrm{excl}}$	2.8
$m_{\mathrm{eff}}^{\mathrm{incl}}$	2.8

Table 25: Cut flow chart for the hard single-lepton 6-jet muon channel. The signal point is taken from the gluino simplified model with $x = 1/2$; 20000 events were generated for this point. The events are normalized to 20.3 fb^{-1}.

Cut	Signal ($m_{\tilde{g}}$ = 1145 GeV, $m_{\tilde{\chi}_1^\pm}$ = 785 GeV, $m_{\tilde{\chi}_1^0}$ = 425 GeV)
Trigger + hard-lepton	18.7
Jets cut	13.0
Jet orthogonality	5.0
$E_{\mathrm{T}}^{\mathrm{miss}}$	2.7
m_{T}	2.3
$E_{\mathrm{T}}^{\mathrm{miss}}/m_{\mathrm{eff}}^{\mathrm{excl}}$	2.3
$m_{\mathrm{eff}}^{\mathrm{incl}}$	2.3

Table 26: Cut flow chart for the hard single-lepton 5-jet electron channel. The signal point is taken from the gluino simplified model with $x = 1/2$; 20000 events were generated for this point. The events are normalized to 20.3 fb^{-1}.

Cut	Signal ($m_{\tilde{g}}$ = 1145 GeV, $m_{\tilde{\chi}_1^\pm}$ = 785 GeV, $m_{\tilde{\chi}_1^0}$ = 425 GeV)
Trigger + hard-lepton	13.0
Jets cut	9.3
Jet orthogonality	3.5
$E_{\mathrm{T}}^{\mathrm{miss}}$	1.7
m_{T}	1.4
$E_{\mathrm{T}}^{\mathrm{miss}}/m_{\mathrm{eff}}^{\mathrm{excl}}$	1.4
$m_{\mathrm{eff}}^{\mathrm{incl}}$	1.4

Table 27: Cut flow chart for the hard single-lepton 5-jet muon channel. The signal point is taken from the gluino simplified model with $x = 1/2$; 20000 events were generated for this point. The events are normalized to 20.3 fb^{-1}.

Cut	Signal ($m_{\tilde{g}}$ = 1145 GeV, $m_{\tilde{\chi}_1^\pm}$ = 785 GeV, $m_{\tilde{\chi}_1^0}$ = 425 GeV)
Trigger + hard-lepton	18.7
Jets cut	18.3
Jet orthogonality	5.4
$E_{\mathrm{T}}^{\mathrm{miss}}$	2.7
m_{T}	2.3
$E_{\mathrm{T}}^{\mathrm{miss}}/m_{\mathrm{eff}}^{\mathrm{excl}}$	1.9
$m_{\mathrm{eff}}^{\mathrm{incl}}$	1.9

Table 28: Cut flow chart for the hard single-lepton 3-jet electron channel. The signal point is taken from the gluino simplified model with $x = 1/2$; 20000 events were generated for this point. The events are normalized to 20.3 fb^{-1}.

Cut	Signal ($m_{\tilde{g}}$ = 1145 GeV, $m_{\tilde{\chi}_1^\pm}$ = 785 GeV, $m_{\tilde{\chi}_1^0}$ = 425 GeV)
Trigger + hard-lepton	13.0
Jets cut	12.8
Jet orthogonality	3.6
$E_{\mathrm{T}}^{\mathrm{miss}}$	1.8
m_{T}	1.3
$E_{\mathrm{T}}^{\mathrm{miss}}/m_{\mathrm{eff}}^{\mathrm{excl}}$	1.0
$m_{\mathrm{eff}}^{\mathrm{incl}}$	1.0

Table 29: Cut flow chart for the hard single-lepton 3-jet muon channel. The signal point is taken from the gluino simplified model with $x = 1/2$; 20000 events were generated for this point. The events are normalized to 20.3 fb^{-1}.

A.4 Signal regions used

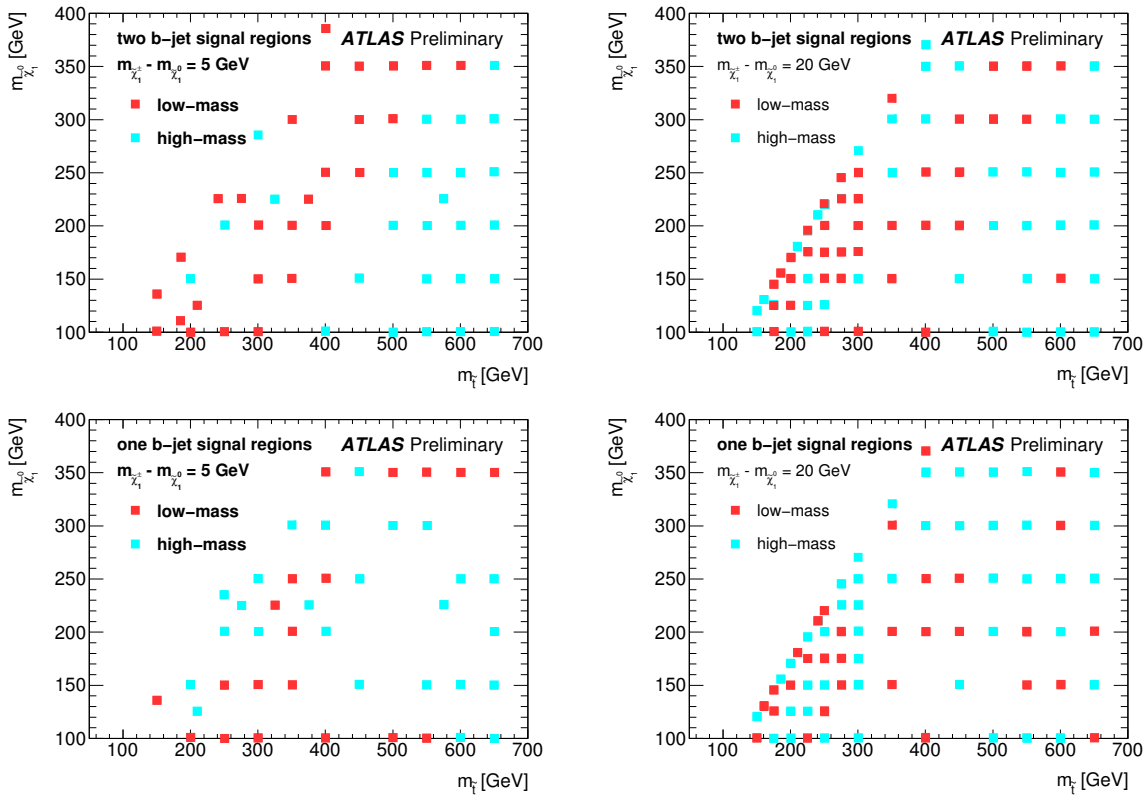

Figure 24: Signal region providing the best expected sensitivity for each point of the top squark pair production simplified model, presented in the $m_{\tilde{t}}$–$m_{\tilde{\chi}_1^0}$ mass plane for the soft single-lepton two b-jet (top) and one b-jet signal regions (bottom) for the case in which the mass difference between the lighter chargino and the LSP is 5 GeV (left) or 20 GeV (right).